INTERIKO 78/7

RADIATION AND SHIELDING AROUND BEAM ABSORBERS

December 1978

A. Hurkmans
R. Maas

RADIATION AND SHIELDING AROUND BEAM ABSORBERS

December 1978

A. Hurkmans
R. Maas

Table of Contents

	p.
1. Geometry and boundary conditions	1
2. Radiation levels at operational conditions	5
2.1 gamma radiation	5
2.2 low-energy neutrons	6
2.3 high-energy neutrons	11
3. Residual activity	17
4. Radiation from copper collimators	27
5. Shielding	31
Appendix. Some useful relations	38
References	45

Shielding around beam absorbers

During operational conditions it should be anticipated that a fair amount of the total available beam power is dumped in either the slit system or one of the beam dumps. These beam absorbers therefore become strong radioactive sources.
In the following pages wewill estimate the radiation level due to the absorption of a 100 kW electron beam of energy $E_0 \lesssim 500$ MeV.
The problem of residual activity (the radiation level under no-beam conditions) will be treated in chapter 3.

1. Geometry and boundary conditions

The slit system consists of the following materials (Fig. 1):

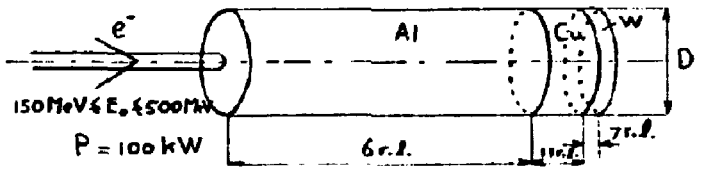

Fig 1

r.l. ≡ radiation length (χ_0)
χ_0 (Cu) = 1.45 cm (13 gcm^{-2})
χ_0 (Al) = 9.0 cm (24.3 gcm^{-2})
χ_0 (W) = 0.35 cm (6.8 gcm^{-2})

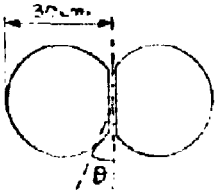

D ∿ 60 cm in the horizontal plane:

In the vertical direction (say $-30^0<\theta<30^0$) D is much smaller. We expect therefore a larger activity in the up- and down directions than in the horizontal directions, see also (5).
Fig. 2 shows the general lay out of the Beam Switch Yard (BSY); a more detailed picture of the slit area is shown in Fig. 3. Collimator C405 is a copper collimator, length ∿25 cm, aperture (X,Y) = (26 mm, 42 mm). Fig. 3 shows clearly, that, as far as radiation hazard is concerned, the positions of both q-poles Q402 and Q403 is critical.
The total activity is due to the contributions from:
a) Gamma's
b) Low-energy (Giant Resonance) neutrons
c) High-energy neutrons

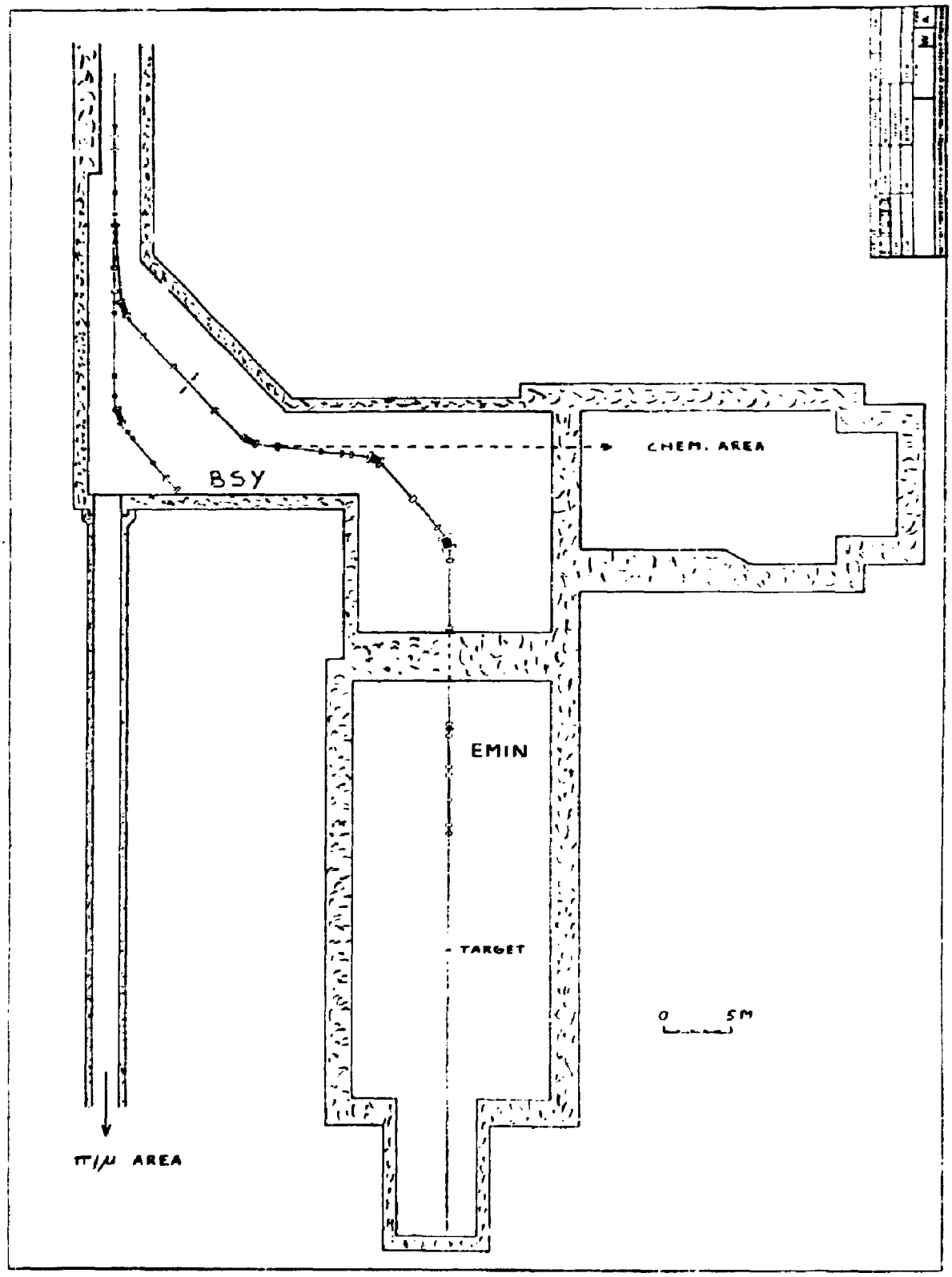

Fig. 2: Building layout showing Beam Switch Yard (BSY), chemist exp. area, high-energy electron scattering area (EMIN), and the tunnel running toward π/μ area.

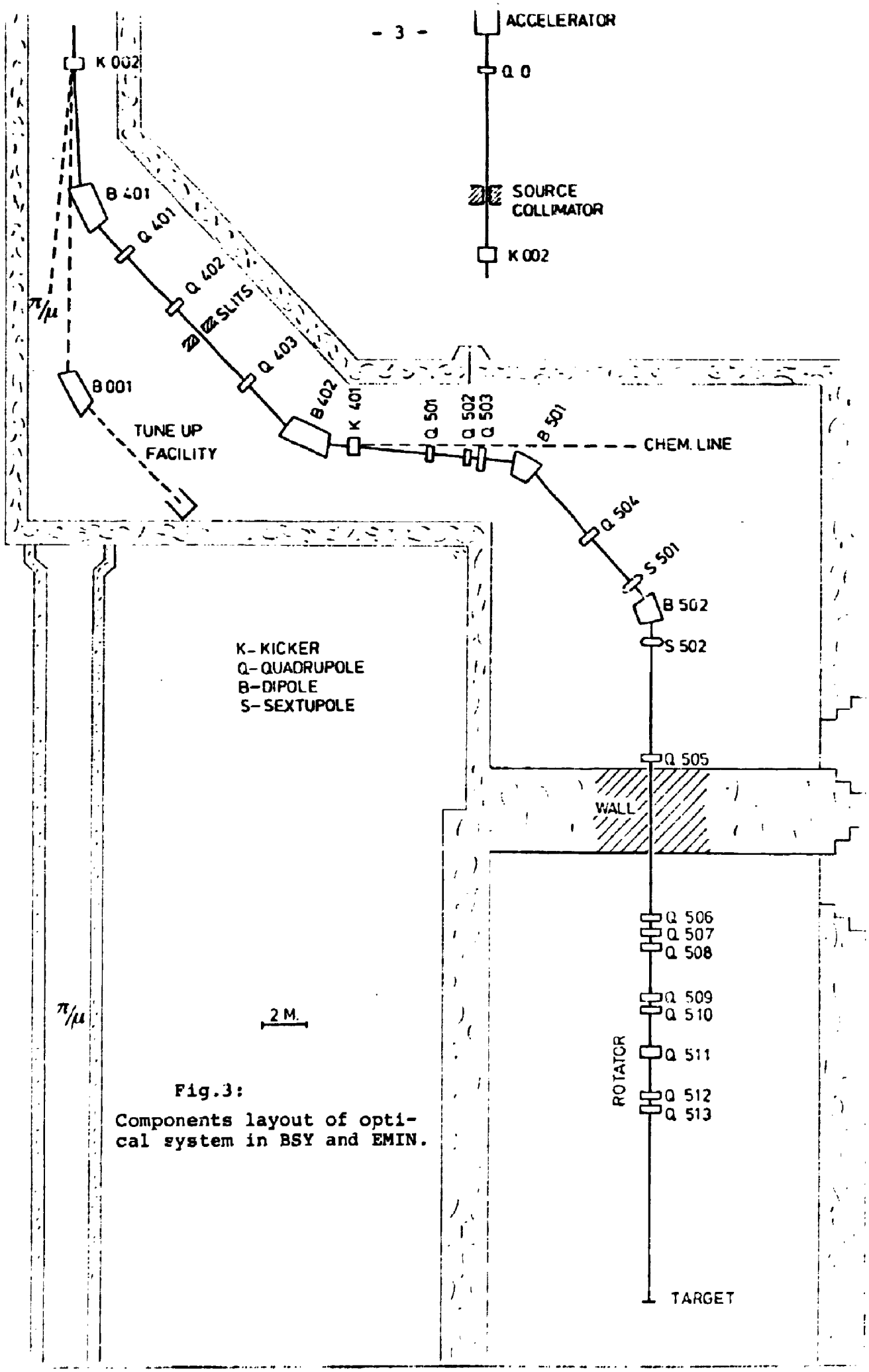

Fig.3:
Components layout of optical system in BSY and EMIN.

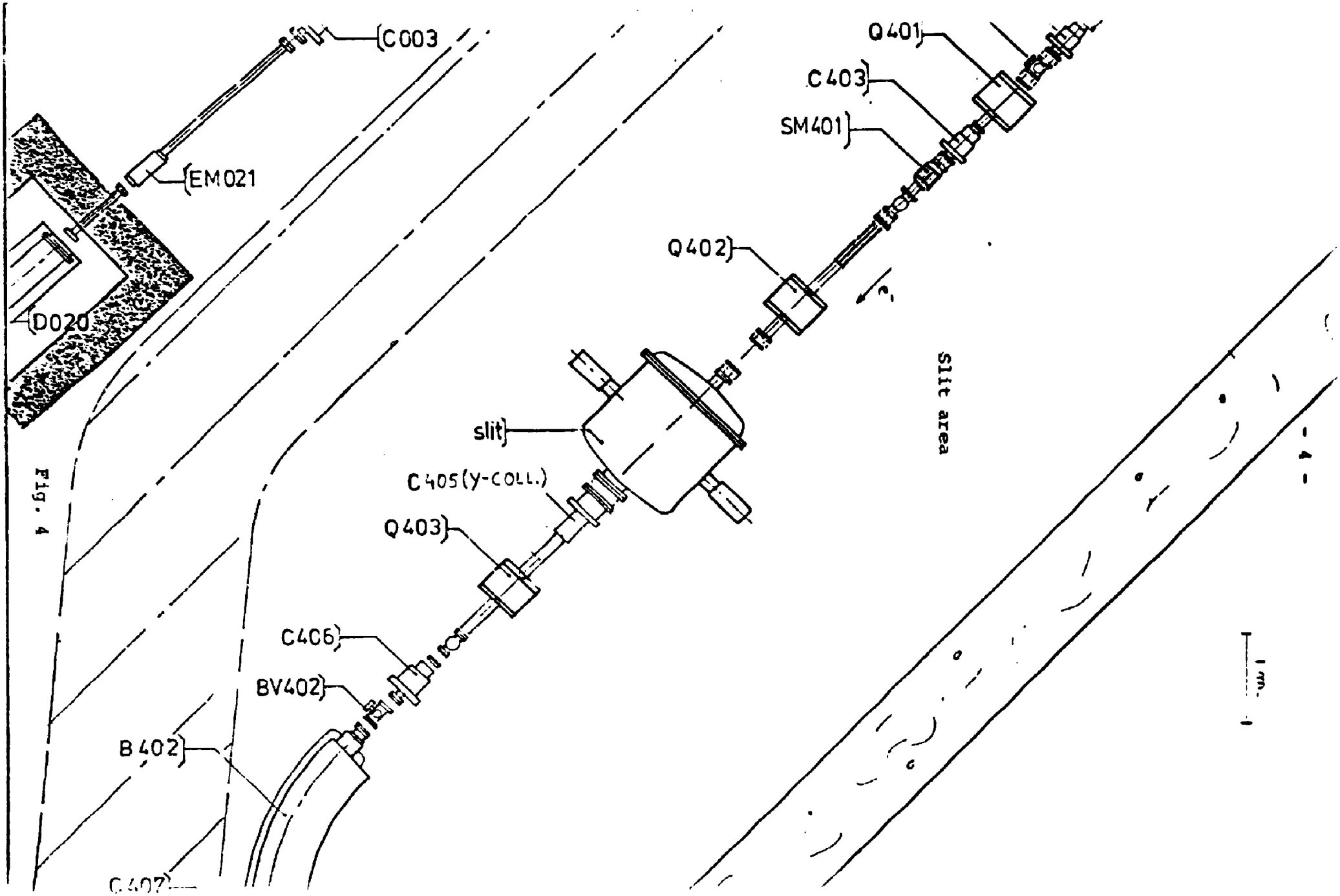
C003
EM021
D020
Q401
C403
SM401
Q402
slit
C405(y-COLL.)
Q403
C406
BV402
B402
C407
slit area
Fig. 4

2. Radiation levels at operational conditions

For the direct radiation due to absorption of beam power we distinguish the following contributions:

a) gamma radiation

b) low-energy neutrons (E_n < 15 MeV)

c) high-energy neutrons (E_n > 15 MeV)

The radiation due to charged particles such as e^- and e^+ is neglected since this type of radiation is shielded very easily compared to the other contributions. High-energy neutrons are most difficult to shield; gamma radiation fairly easy.

2.1 Gamma radiation

The contribution of the photon dose rate from the slits is given sufficiently accurate in Fig. 5, where the dose rate per kW absorbed beam power is plotted versus angle. The photon dose rate is given for an electron beam of 1 kW power, incident on a solid copper (1,2) and iron (2) cylinder respectively. The dimensions of the cylinders were approximately 3-4 Molière units [+], X_m(1), radially and 15-20 radiation lengths (r.l.) axially. The dimensions of the slit modules fall, more or less, within this range.
In axial direction the system consists of (see Fig. 1): a module filled with aluminium spheres of 6 r.l., a copper absorber of 11 r.l. and a tungsten plate of 10 r.l. The tungsten plate can be considered as an extra absorber in forward direction: this reduces the forward flux by a factor 14 [++] compared to an absorber of axial length 15-20 r.l. as used in Fig. 5, giving 1.4 10^6 rad. h^{-1} per 100 kW at 1 m distance.

+) The Molière unit is given by $X_m = X_0 . E_s/\varepsilon_0$ with E_s = 21.2 MeV and ε_0 the critical energy for the absorber. (ε_0) = MeV, (X_0) = $g\,cm^{-2}$

++) The minimum absorption coefficient for tungsten is estimated by interpretation of data given by Crannel et al. (3,4):

$\xi_w \sim 0.04\ cm^2 g^{-1}$; $\rho_w = 19.3\ g\,cm^{-3}$; $\mu = \xi \cdot \rho = 0.77\ cm^{-1}$

$e^{-\mu t\,[cm]} = e^{-0.77 * 3.5} = 0.07$.

The "radial" length in the horizontal plane consists of 20 cm aluminium which gives 4.1 X_m. This is exactly the radial length as in measurements performed by Neet (2). From this we find for the transverse ($\theta = 90^\circ$) radiation in the horizontal plane: 10^5 rad hr^{-1} per 100 kW at 1 m distance.
In the vertical plane the radial length is 2.1 X_m. The radiation in this plane is therefore higher than in the horizontal plane: a factor 4 to 5 +).

Summarizing, we find the following contributions of gamma radiation at 1 m distance for an electron beam with E_0 = 500 MeV and P = 100 kW, which is completely absorbed in the slit system:

i) Forward radiation : $D_F = 1.4\ 10^6$ rad hr^{-1}
ii) Transverse radiation in the horizontal plane : $D_{TH} = 1 \cdot 10^5$ rad hr^{-1}
iii) Transverse radiation in the vertical plane : $D_{TV} = 5 \cdot 10^5$ rad hr^{-1}

2.2 Low-energy neutrons

The neutrons from the radiation field are produced nearly exclusively by the interaction with the absorber material of photons, which are emitted by the electrons in an electromagnetic cascade within the absorber. Neutrons from the Giant Resonance consitute the major part in the energy spectrum of the emitted neutrons. Their maximum energy is approximately 20 MeV, average energy a few MeV.

+) Comparing the fraction of energy escaping from a cylinder (see Fig. 26.2, ref. 1) with $r_0/X_m = 3.1$ and $r_0/X_m = 4.1$ respectively gives a factor 4 reduction. In a previous report on the slit-system (5) we estimated the angular distribution of power escaping from the slit modules. From this, integrating over 30 degr, we find a factor 5.

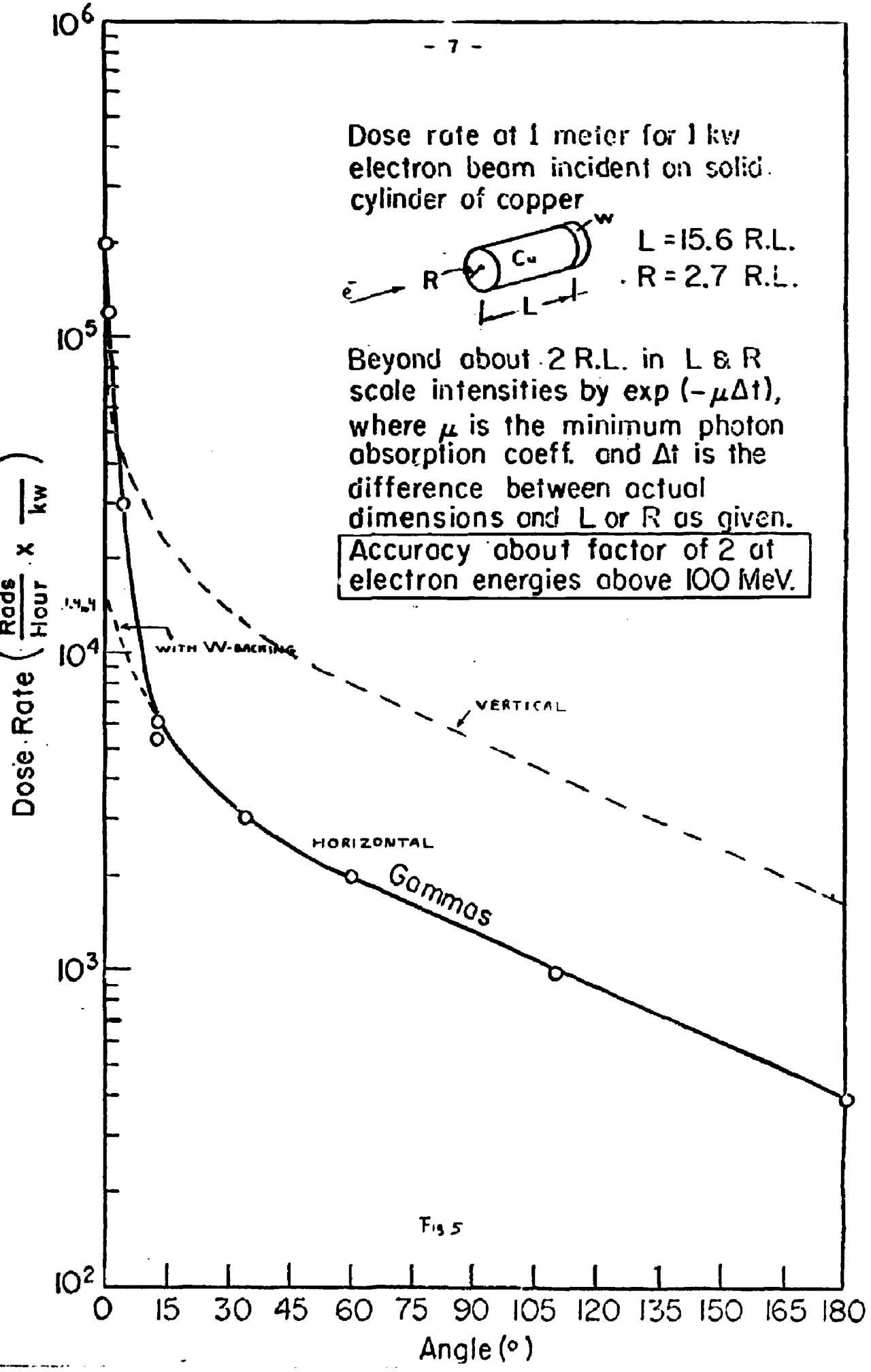
Dose rate at 1 meter for 1 kw electron beam incident on solid cylinder of copper
W
Cu
R
e⁻
L
L = 15.6 R.L.
R = 2.7 R.L.
Beyond about 2 R.L. in L & R scale intensities by exp (−μΔt), where μ is the minimum photon absorption coeff. and Δt is the difference between actual dimensions and L or R as given.
Accuracy about factor of 2 at electron energies above 100 MeV.
WITH W-BACKING
VERTICAL
HORIZONTAL
Gammas
Dose Rate (Rads/Hour x 1/kw)
10⁶
10⁵
10⁴
10³
10²
0 15 30 45 60 75 90 105 120 135 150 165 180
Angle (°)

Fig 5

The photo-neutron yield is obtained by the integration of the photon differential track length $dL^{\gamma}(E_0,k)/dk$:

$$Y(E_0) = \frac{N_0 \rho}{A} \int_{k_{th}}^{E_0} \sigma_n(k) \frac{dL^{\gamma}(E_0,k)}{dk} dk \qquad (2.1)$$

$Y(E_0)$ gives the number of neutrons per incident electron,

E_0 : the incident electron kinetic energy,

N_0 : Avogadro's number,

ρ : density,

A : atomic weight,

$\sigma_n(k)$: photo-neutron cross section,

k : photon energy,

k_{th} : threshold energy for the Giant Resonance process (in the range 6-13 MeV for most materials).

The photon differential track length is evaluated in the literature in three different manners:

1) Approximation A of shower theory.
   Physical processes: bremsstrahlung and pair production.
2) Approximation B of shower theory.
   Physical processes: bremsstrahlung, pair production and ionization loss..
3) Monte Carlo calculations.
   Many physical processes can be implemented in the computer cascade-transport code.

In approximation A of shower theory (6), where only bremsstrahlung and pair production are taken into account, the photon differential track length is given by:

$$\frac{dL^{\gamma}}{dk} = 0.572 \frac{E_0 X_0}{k^2} \qquad (2.2)$$

where X_0 is the radiation length.

Substitution into eq. 2.1 and evaluation of the numerical constants yields

$$Y_{GR}[n\,sec^{-1}/e^{-}] = 3.4_{10}23 \frac{E[MeV]\ X_o[g\,cm^{-2}]}{A} \int_{G.R.} \frac{\sigma(k)}{k^2}\,dk\ [cm^2.MeV^{-1}] \qquad (2.3a)$$

Since the photo-neutron cross section is peaked rather pronouncedly in the Giant Resonance region, especially for large Z, we may write:

$$Y_{GR}[n\,sec^{-1}/e^{-}] = 3.4_{10}23 \frac{E[MeV]\ X_o[g\,cm^{-2}]}{A} \frac{1}{k^2_{GR}\,[MeV^2]} \int_{G.R.} \sigma(k)dk\ [cm^2.MeV] \qquad (2.3b)$$

or, which is equivalent,

$$Y_{GR}[n\,sec^{-1}] = 2.13_{10}39 \frac{P[kW]\ X_o[g\,cm^{-2}]}{A} \frac{1}{k^2[MeV^2]} \int_{GR} \sigma(k)\,dk\,[cm^2.MeV] \qquad (2.3c)$$

A numerical evaluation of the yield of Giant Resonance neutrons for some materials is given in table I.

Swanson (7) used approximation B of analytical shower theory (6,8) to calculate the yield of Gaint Resonance neutrons. In approximation B, apart from bremsstrahlung and pair production, the energy loss by ionization is taken into account. The results of these calculations are given in table I and compared with the approximation A calculations. Swanson found the following Z-dependence for high energies E (E large compared to the critical energy ε_0) as a result of a "least squares fit" to his calculations:

$$Y[n\,sec^{-1}kW^{-1}] = 9.3_{10}10\ Z^{0.73\pm0.05} \qquad (2.4a)$$

or

$$D[REM.hr^{-1}kW^{-1}] = 93\ Z^{0.73\pm0.05}/d^2[m^2] \qquad (2.4b)$$

Table I: Some data for Giant Resonance neutrons emitted from different absorber materials. The yields have been calculated for the absorption of 1 kW of electron beam power under approximation A and approximation B respectively of shower theory.

					APPROXIMATION A		APPROXIMATION B	
							Swanson (d); E_0 = 500 MeV	
material	A	X_0 (gcm^{-2})	k_{GR} (MeV)	$\int_{GR} \sigma dk$ (MeV.barn)	Y_{GR} ($nsec^{-1}kW^{-1}$)	Dose equiv. ($mrem.hr^{-1}kW^{-1}$) at r = 1m	Y_{GR} ($nsec^{-1}kW^{-1}$) (d)	Dose equiv. ($mrem.hr^{-1}kW^{-1}$) at r = 1m
C	12	44.6	22.9	0.042 (a)	$0.63\ 10^{12}$	$7.1\ 10^{5}$	$0.38\ 10^{12}$	$3.8\ 10^{5}$
H_2O	16(b)	37	21.5	0.150 (b)	$1.6\ 10^{12}$	$1.8\ 10^{6}$		
Al	27	24.3	19.2	0.045 (a)	$0.23\ 10^{12}$	$2.6\ 10^{5}$	$0.56\ 10^{12}$	$6\ 10^{5}$
Fe	56	14.1	18.7	0.48 (a)	$0.74\ 10^{12}$	$8.2\ 10^{5}$	$0.76\ 10^{12}$	$8\ 10^{5}$
Cu	63.5	13	17	0.80 (a,c)	$1.2\ 10^{12}$	$1.3\ 10^{6}$	$1.08\ 10^{12}$	$1.1\ 10^{6}$
Ta	181	6.5	15	5.00 (c)	$1.7\ 10^{12}$	$1.9\ 10^{6}$	$2.13\ 10^{12}$	$2.1\ 10^{6}$
Au	197	6.6	13.9	3.19 (a)	$1.2\ 10^{12}$	$1.3\ 10^{6}$	$2.13\ 10^{12}$	$2.1\ 10^{6}$
Pb	207	6.5	13.7	4.8 (a)	$1.7\ 10^{12}$	$1.9\ 10^{6}$	$1.98\ 10^{12}$	$2.0\ 10^{6}$

(a) M. Pelliccioni, IEEE Trans. Nucl. Sc. 23 (1976) 1344.

(b) Data for O^{16}: H. De Staebler, "Photon-Induced Residual Activity", SLAC-TN-63-92 (1963).

(c) J.L. Matthews, Shielding Note No 6, Nov. 1967, Lab. for Nucl. Science.

(d) Calculations for E_0 = 500 MeV by W.P. Swanson, Health Phys. 35 (1978) 353.

We will use the rule of thumb (2.4b) for the calculation of the flux of Giant Resonance neutrons (low-energy neutrons). The power of the electron beam is absorbed mainly (90%) in the aluminium slit modules. Then, in case of absorption of the full 100 kW beam, we find at a distance of d = 1m from the slits:

$$D = 6 \times 10^{4} \text{ rem.hr}^{-1}.$$

2.3 High-energy neutrons

The radiation field after a thick concrete wall can be considered as consisting of merely high-energy neutrons. The effective dose D after a thick concrete wall is estimated by a semi-empirical formula given by Mulder (9) who used measurements of 1.1 GeV electrons absorbed in copper:

$$D_{PL}\,[\text{mrem hr}^{-1}\text{kW}^{-1}] = 6{,}10^{4}\ \frac{X_o^m}{X_o^{Cu}}\ e^{-\frac{\varrho t}{\lambda}} \Big/ r^2\,[\text{m}^2] \qquad (2.5)$$

where D_{PL} is the dose in forward direction for a point source, X_0^m and X_0^{Cu} (gcm^{-2}) the absorber radiation lengths for material m and Cu respectively, λ (gcm^{-2}) is the mean free path of the neutrons, ρ (gcm^{-3}) is the density, t (cm) the thickness of the shield and r (m) is the distance to the source.
For an aluminium absorber and a concrete shield:

$$D_{PL}\,[\text{mrem hr}^{-1}\text{kW}^{-1}] = 1{,}1\ 10^{5}\ e^{-0.022\,t\,[\text{cm}]} \Big/ r^2\,[\text{m}^2] \qquad (2.6)$$

The yield of photoneutrons can be described using the simple effective deuteron model (10,11,12). This model is valid for not too large energies, so that the contribution of pion reactions can be neglected. Then, (approximation A):

$$Y_H = 0.57\ \frac{E_o\, X_o\, N_o}{A} \int_{k_{min}}^{E_o} \frac{1}{k^2}\, \sigma_{qd}(k)\, dk \qquad (2.7)$$

where σ_{qd} represents the quasi-deuteron cross section which can be written as: σ_{qd} (nucleus) = K.A. σ_{exp} (deuteron).
K.A. gives the effective number of deuterons in the nucleus with
$K = \alpha \frac{(A-Z)Z}{A^2}$
the constant α ranges between 1.5 and 4 (10, 11, 12).
Using the experimental cross section:

$$\sigma_{exp} \text{ (deuteron)} = 60 \quad \mu b \quad k < 300 \text{ MeV}$$
$$\sigma_{exp} \text{ (deuteron)} = 60 \left[\frac{300}{k}\right]^2 \mu b \quad k > 300 \text{ MeV}$$

and α = 4 (10,11), eq.(2.3.2) becomes: (E_o in MeV)

$$\left.\begin{aligned} Y_H\,[n\,sec^{-1}] &= 1.25_{10}11\ X_o\,[g\,cm^{-2}]\ P[kW]\left(\frac{1}{k_{min}} - \frac{1}{E_o}\right) \quad , E_o \leq 300\ MeV \\ Y_H\,[n\,sec^{-1}] &= 1.25_{10}11\ X_o\,[g\,cm^{-2}]\ P[kW]\left(\frac{1}{k_{min}} - 2.22_{10}{-3} - \frac{3_{10}4}{E_o^3}\right), E_o > 300\ MeV \end{aligned}\right\} \quad (2.8)$$

Matthews (11) proposed to use k_{min} = 40 MeV. For aluminium, in case of 100 kW absorption, we find:

$$Y_H^{AL}\ (nsec^{-1}) = 6.9\ 10^{12}\ (\sim 1.6\ 10^7\ mrem\ hr^{-1}\ at\ r = 1m).$$

Detailed calculatins have been performed by Gabriel and Alsmiller (13) who used a Monte-Carlo technique to compute the photoneutron yield in the electron-photon cascade process for 400 MeV electrons incident on a thick Cu target. In their calculations bremsstrahlung, continuous slowing down, small-angle Coulomb scattering and large angle Coulomb scattering of electrons and positrons, were taken into account.
The interactions with matter of the photons was described by pair production, Compton scattering and photo-ionization. Results of those calculations are shown in the histrograms of Figs. 6a and 6b. These data have been used to calculate the dose equivalent rate D of the emitted fast neutrons per incident electron, as follows:

$$D[\text{mrem hr}^{-1}/e^-] = \frac{10^{-4}}{r^2} \sum_i c(E_i) \left(\frac{d^2n}{dE\,d\Omega}\right)_{E_i} \Delta E_i \qquad (2.9)$$

the differential yield per incident electron $Y_i \equiv (\frac{d^2n}{dEd\Omega})_{E_i}$ is given in Fig. 6a and Fig. 6b for Cu at energy E_i and energy bin ΔE_i. The conversion factor for fluence rate to dose equivalent $c(E_i)$ (mrem $hr^{-1}/(ncm^{-2}sec^{-1})$) is given in table A1. Since the distance r is given in m, we have to multiply with 10^{-4}. According to eq. (2.8) the yield of fast photoneutrons scales with the radiation length. For aluminium we may therefore write: $Y_i^{Al} = (X_0^{Al}/C_0^{Cu}).Y_i$.
Evaluation of eq. (2.9) for aluminium and 100 kW beam power yields at r = 1m:

Forward angles (0-30°) $D_F^{Al} = 2.5\ 10^7$ mrem hr^{-1}

Transverse (∿90°) $D_T^{Al} = 1.5\ 10^7$ mrem hr^{-1}

The angular distribution of the dose equivalent rate and the fluence rate of neutrons which are emitted after absorption of 1 kW of electrons with approximately 400 MeV energy, is shown in Fig. 7. The angular distribution is almost isotropic. However, it should be noted that concrete shielding attenuates the dose rate due to low-energy (GR) much more than the dose rate due to high-energy neutrons. Therefore, in case of thick concrete shielding (>1m) one can neglect the contribution from low-energy neutrons, indicated in Fig. 7 with dashed lines.

Summarizing, the total radiation field at 1 m from the slits in case of absorption of the full 100 kW, 500 MeV electron beam, consists of:

Forward radiation:	gamma radiation	$1.4\ 10^6$ rad hr^{-1}
	low-energy neutrons	$6\ 10^4$ rem hr^{-1}
	high-energy neutrons	$2.5\ 10^4$ rem hr^{-1}
Transverse radiation:		
- horizontal plane:	gamma radiation	10^5 rad hr^{-1}
	low-energy neutrons	$6\ 10^4$ rem hr^{-1}
	high-energy neutrons	$1.5\ 10^4$ rem hr^{-1}
- vertical plane:	gamma radiation	$5\ 10^5$ rad hr^{-1}
	low-energy neutrons	$6\ 10^4$ rem hr^{-1}
	high-energy neutrons	$1.5\ 10^4$ rem hr^{-1}

Differential neutron yield from 400 MeV electrons incident on Cu.
Differential yield, Y, in (neutrons)/(sterad.MeV.incident e^-), ref (13).

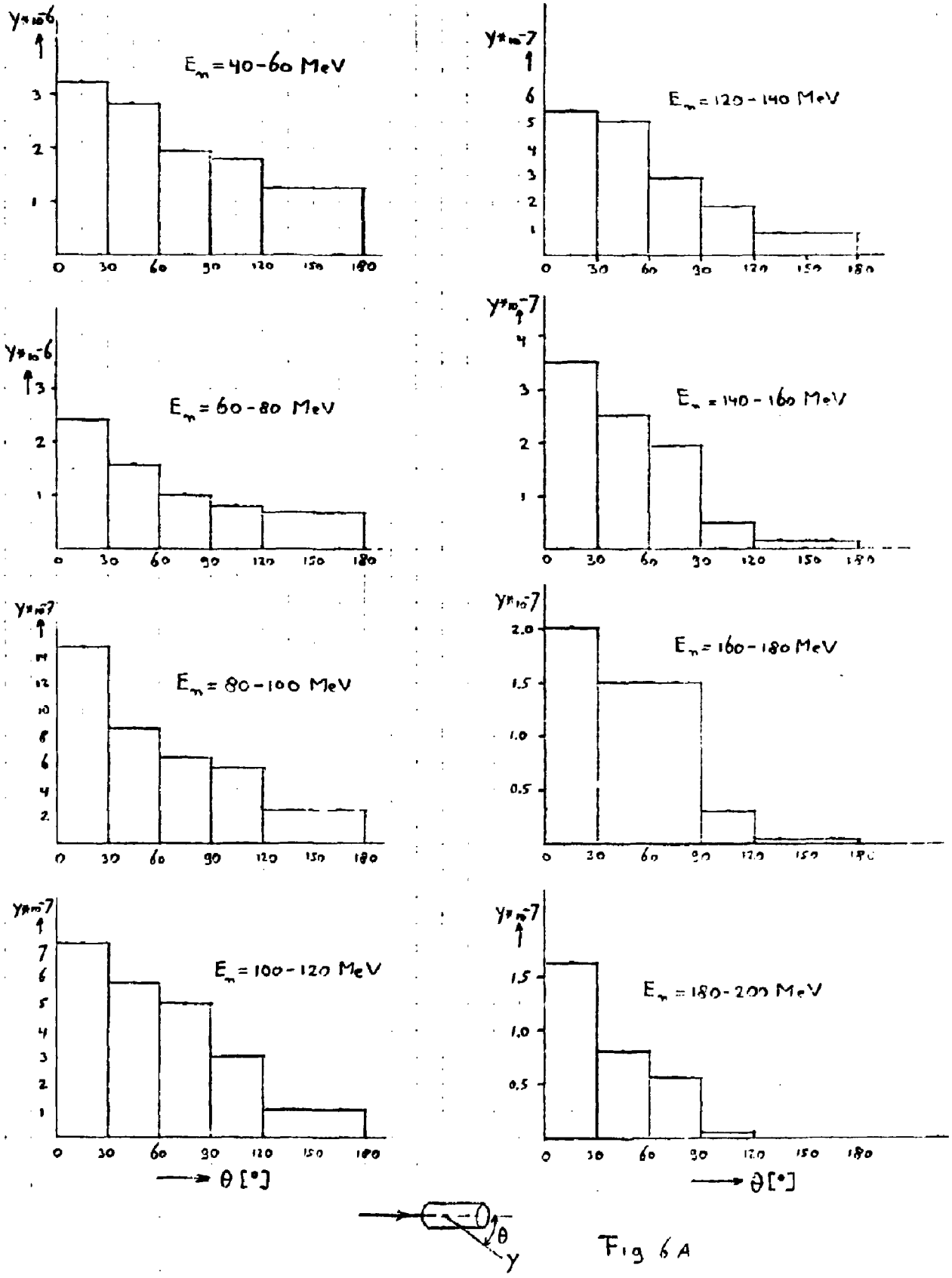

Fig 6A

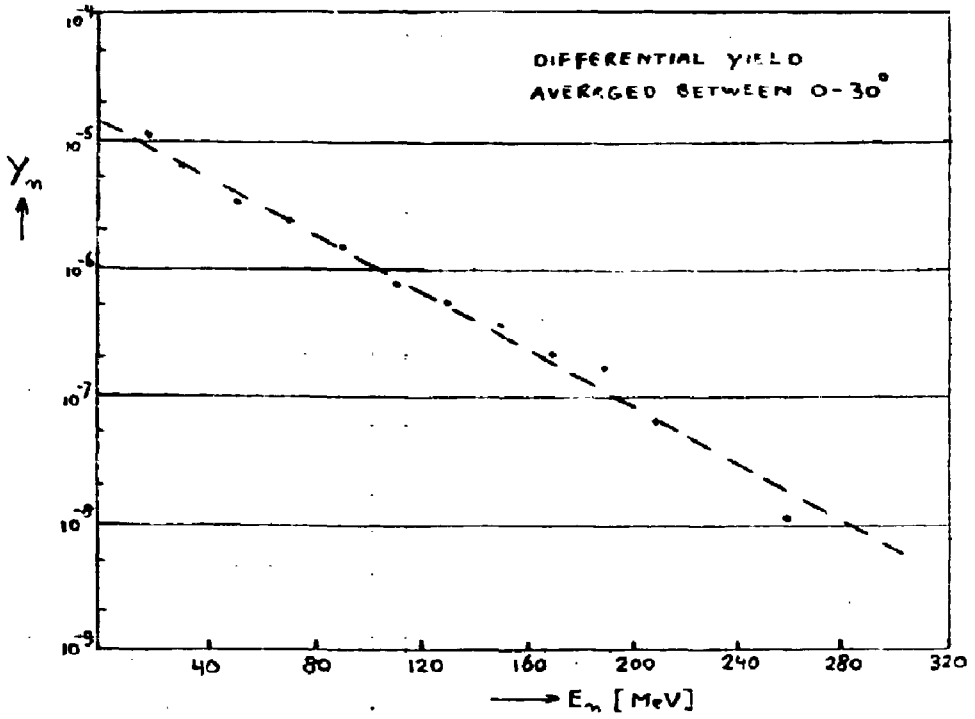

Differential yield, Y_n, of neutrons (n/(sterad.MeV.e^-)) from 400 MeV electrons incident on a thick Cu target, ref (13).

Fig. 6b

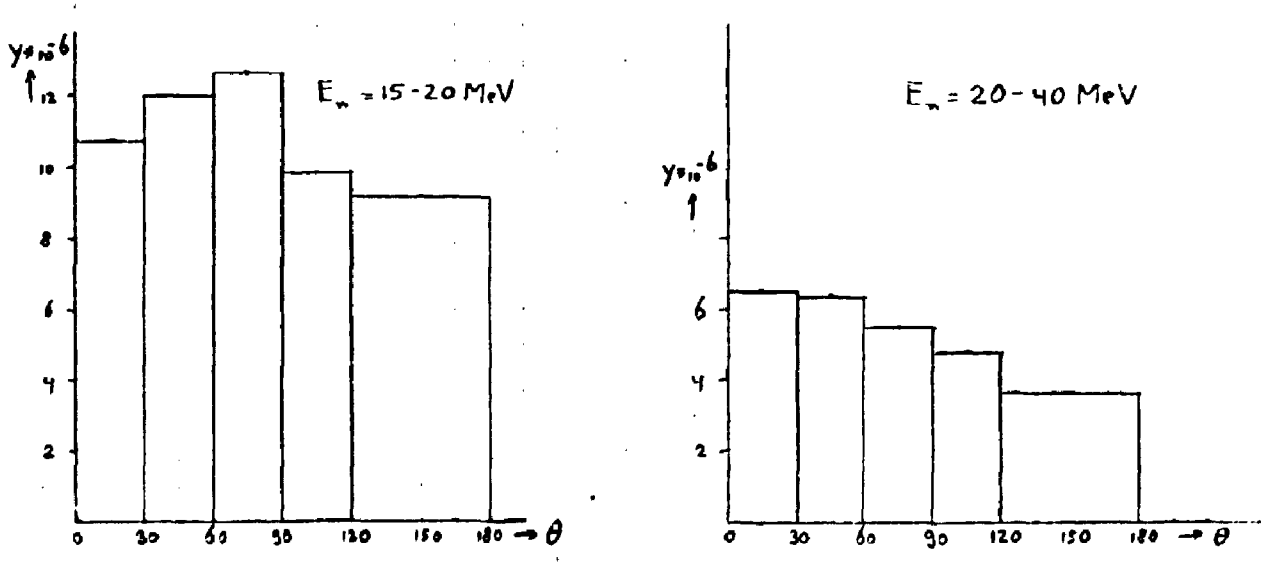

Differential neutron yield from 400 MeV electrons incident on Cu. Differential yield, Y, in (neutrons)/(sterad.MeV.incident e^-).

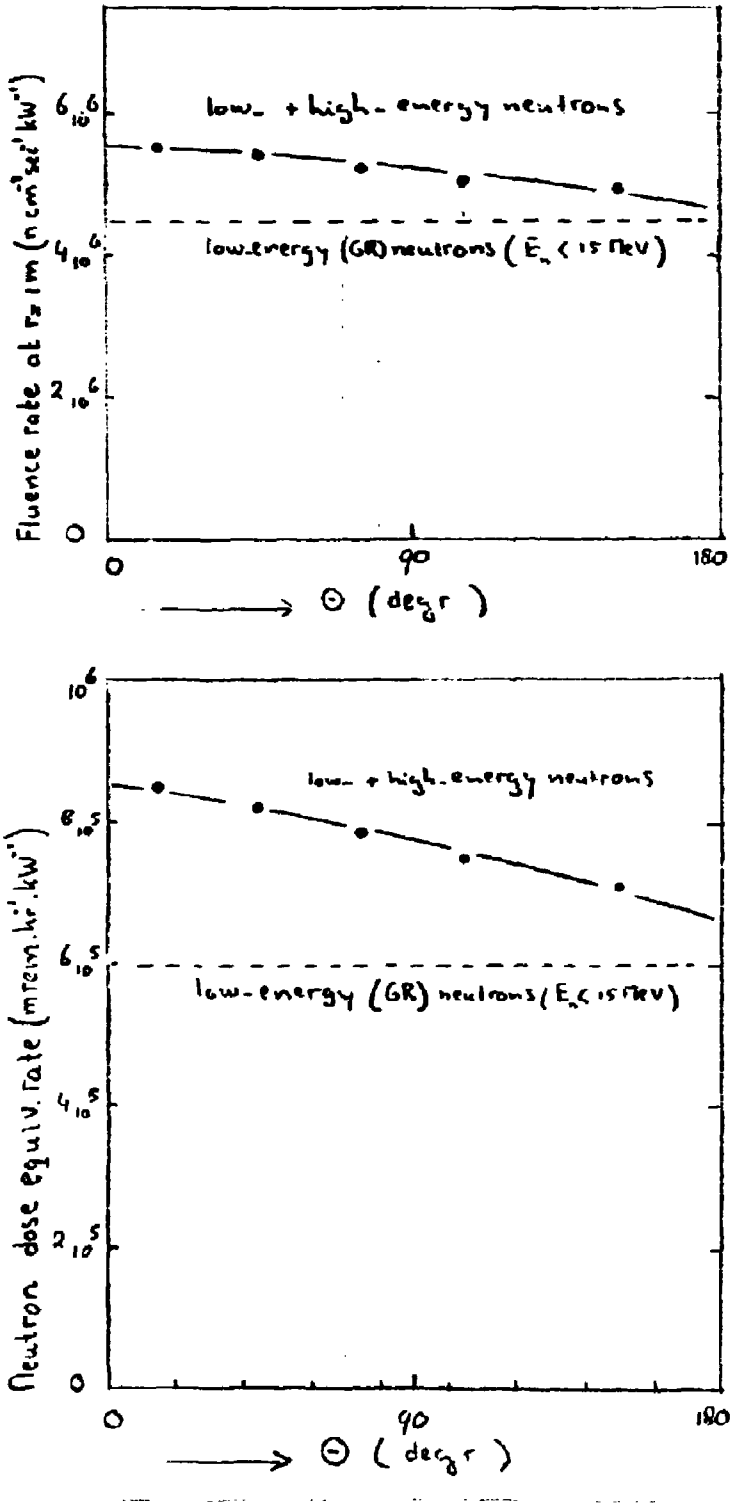

Fig. 7: Neutron fluence rate and neutron dose equivalent rate at 1m distance from an aluminium absorber after bombardment of 1 kW electron beam with $E_0 \sim 400$ MeV. Calculations for low-energy neutrons from data by Swanson (7); for fast neutrons from data by Gabriel and Alsmiller (13).

3. Residual Activity

After beam shut-off the slit/dump system can be considered as a radioactive source. The bulk of the radiation consists of gamma's, $E_\gamma \lesssim 2$ MeV. Most of the emitted electrons are stopped by self-shielding of the device:

range $R(E_e = 1\ \text{MeV}) = 4.4$ mm
$R(E_e = 2\ \text{MeV}) = 2.4$ mm for Aluminium

Both the slit system and the dumps consist of aluminium(and water) and copper. Roughly 90% of the total beampower is absorbed in the Al-water part and 10% in the Cu-part. The isotopes which contribute mostly to the residual activity are:

^{22}Na; $\tau_{\frac{1}{2}} = 2.62$ yr
^{24}Na; $\tau_{\frac{1}{2}} = 15$ hr from Al part

---

^{61}Cu; $\tau_{\frac{1}{2}} = 3.3$ hr
^{64}Cu; $\tau_{\frac{1}{2}} = 12.7$ hr from Cu part

The contribution of ^{22}Na will manifest itself as a, practically constant, background (with a magnitude proportional to $\Sigma|P(\text{DISSIPATED}) * t(\text{DAYS})|$). The saturation activity, $\dot{X}_s$, is given by (17)

$$\dot{X}_s\,[R\cdot hr^{-1}m^{-2}] = 5.8_{10}{}^{-2}\ P[kW]\ \frac{\chi_0\,[g\,cm^{-2}]}{A}\ \sigma_{-2}[\mu b\cdot MeV^{-1}]\ \Gamma\,[R\cdot hr^{-1}m^{2}Ci^{-1}] \qquad (3.1)$$

P is incident power
χ_0 radiation length

$$\sigma_{-2} = \int_0^{E_{max}} \frac{\sigma(E_\gamma)}{E_\gamma^2}\, dE_\gamma$$

Γ specific gamma ray constant (conversion from curie to $R.hr^{-1}\ m^{-2}$)

'Contribution from Aluminium part

Al: $\chi_0 = 23.3\ gcm^{-2}$

A = 27

P ∿ 90 kW (3.1) $5.8_{10}{}^{-2} * 90\ \frac{23.9}{27} * 1.84 = 8.50$, so

DISTANCE r = 1m

F(^{24}Na) = 1.84 (3.1) reduces to:

$$\dot{X}_5[R\cdot hr^{-1}] = 8.50\ \sigma_{-2}[\mu b\cdot MeV^{-1}] \qquad (3.2)$$

According to Swanson (17),

$$\sigma_{-2}(^{24}Na) \equiv \int_0^{19\,GeV} \frac{\sigma(E_\gamma)}{E_\gamma^2}\, dE_\gamma = 5.4\ \mu b\cdot MeV^{-1} \qquad (3.3)$$

Since we are interested in $\int_{30\ à\ 40\ MeV}^{500\ MeV}(\sigma/E^2)dE$, we estimate the effect of this truncation from the σ_0-determination of Meyer et al. (14). These authors studied the reaction $^{27}Al(\gamma, 2pn)^{24}Na$:

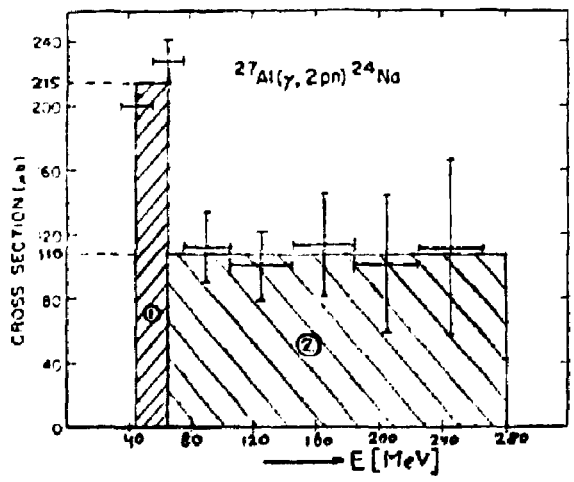

$$\sigma_0 \equiv \int_0^{E_{max}} \sigma dE$$

for $E_{max} \sim 275$ MeV, Meyer et al. deduced $\sigma_0 = 31 \pm 3.3$ mb.MeV. Since σ is nearly constant in the two indicated regions, ① & ②, this result can easily be checked:

$$\left.\begin{aligned} &\int_{40}^{65}\sigma(1)\,dE \sim 0.215\,(65-40) = 5.4\ \text{mb·MeV} \\ &\int_{65}^{300}\sigma(2)\,dE \sim 0.110\,(275-65) = 23.1\ \text{mb·MeV} \end{aligned}\right\} \sigma_0 = 28.5\ \text{mb·MeV}$$

In order to evaluate the value of σ_{-2}, we follow essentially the same procedure:

$$\sigma_{-2} = \int_{E_1}^{E_2}(\sigma/E^2)\,dE \sim \sigma\int_{E_1}^{E_2} dE/E^2 = \sigma\left(\frac{1}{E_1} - \frac{1}{E_2}\right)$$

, so

$$\left.\begin{aligned} &\sigma_{-2}(1) = 215\left(\tfrac{1}{40} - \tfrac{1}{65}\right) = 2\ \mu\text{b·MeV}^{-1} \\ &\sigma_{-2}(2) = 110\left(\tfrac{1}{65} - \tfrac{1}{300}\right) = 1.3\ \text{"} \end{aligned}\right\} \Rightarrow \sigma_{-2} = 3.3\ \mu\text{b·MeV}^{-1}$$

This σ_{-2}-value substituted into (3.2) yields finally

$$\dot{X}_s\,[\text{R·hr}^{-1}] = 8.50 * 3.3 = 28\ \text{R·hr}^{-1} \qquad (3.4)$$

(3.4) is in agreement with calculations of J. Visser (15); the latter calculations are based upon $\sigma_q = \sigma_{-1} \equiv \int_0^{E_{max}}(\sigma/E)\,dE$. From (15): $\sigma_q(\text{Al})^{E=400\ \text{MeV}} \sim 0.5$ mb; by using $\sigma_{-2} \sim \frac{1}{E}\sigma_q$, we find $\sigma_{-2} \sim \frac{1}{100\ \text{MeV}}\ 0.5\ \text{mb} = 5\ \mu\text{b.MeV}^{-1}$.

Contribution from Copper part

$$\text{Cu: } \text{NAT}_{\text{Cu}} \quad \begin{matrix}70\%\ ^{63}\text{Cu} \\ 30\%\ ^{65}\text{Cu}\end{matrix} \quad P_{tot}(\text{Cu=10kW}) \quad \begin{matrix}P\ (^{63}\text{Cu}) = 7\ \text{kW} \\ P\ (^{65}\text{Cu}) = 3\ \text{kW}\end{matrix} \qquad (3.5)$$

$$\chi_0 = 13\ \text{gcm}^{-2}$$

The active isotopes which are of concern here, ^{61}Cu and ^{64}Cu, are produced by the reactions: $^{63}Cu(\gamma,2n)^{61}Cu$, see ref. (16)
$^{65}Cu(\gamma,n)^{64}Cu$, see ref. (18)

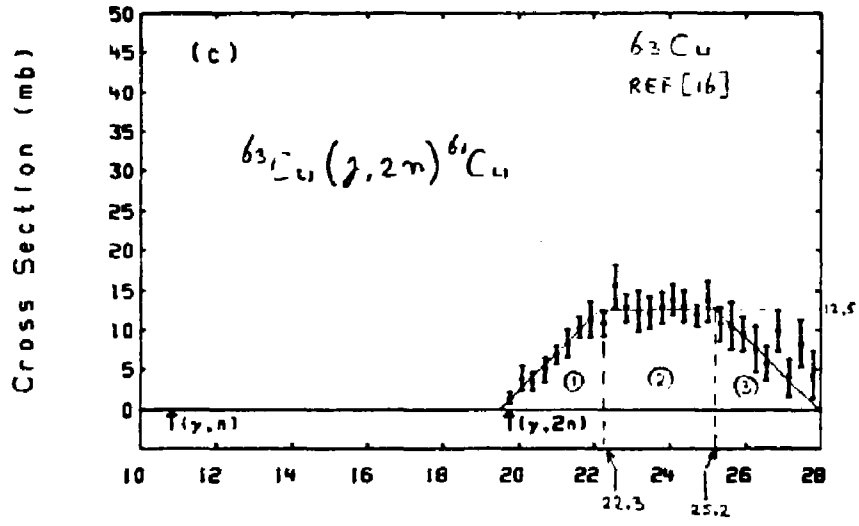

Fig 9

We divide the spectrum into three parts, ①, ② and ③ and evaluate for each part $(\sigma/\bar{E}^2)\Delta E$:

(1) $\left\{\left(\frac{12.5}{2}\right)/\left(\frac{22.3+20}{2}\right)^2\right\}(22.3-20) = \frac{6.25}{(21.15)^2}\,2.3 = 3.2_{10}{-2}$ mb.MeV^{-1}

(2) $\left\{12.5/\left(\frac{25.2+22.3}{2}\right)^2\right\}(25.2-22.3) = \frac{12.5}{(23.8)^2}\,2.9 = 6.4_{10}{-2}$ " "

(3) $\left\{\left(\frac{12.5}{2}\right)/\left(\frac{28+25.2}{2}\right)^2\right\}(28-25.2) = \frac{6.25}{(26.6)^2}\,2.8 = 2.5_{10}{-2}$ " "

$12.1_{10}{-2}$ mb.MeV^{-1} +

$$\Rightarrow \sigma_{-2}\left(^{63}Cu(\gamma,2n)^{61}Cu\right) \sim 120\,\mu b.\,MeV^{-1} \qquad (3.6)$$

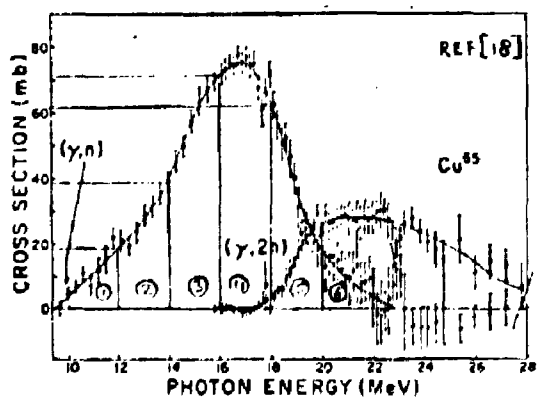

Fig. 10. Partial cross sections for Cu^{65}. The top curve consists of $\sigma(\gamma,n)+\sigma(\gamma,np)$. The lower curve consists of $\sigma(\gamma,2n)$ and was obtained from double neutron counting data.

The same technique has been applied to evaluate $\sigma_{-2}(\gamma,n)$ for ^{65}Cu. The result is:

$\sigma_{-2}(^{65}Cu(\gamma,n)^{64}Cu) \sim$

~ 1.70 mb. MeV^{-1} (3.7)

The Γ-values, see (3.1), are obtained from (19):

$$\Gamma(^{61}Cu) = 0.4$$
$$\Gamma(^{64}Cu) = 0.1 \qquad (3.8)$$

Substitution of (3.5), (3.6), (3.7) and (3.8) into (3.1) yields:

$$\dot{X}_s(^{61}Cu) = 5.8_{10}{-2} * 7 * \frac{13}{61} * 120 * 0.4 = 4.15 \ R \cdot hr^{-1}$$

$$\dot{X}_s(^{64}Cu) = 5.8_{10}{-2} * 3 * \frac{13}{64} * 1700 * 0.1 = 6.01 \ R \cdot hr^{-1}$$

$$\Rightarrow \qquad \dot{X}_s(Cu) \sim 10 \ R \cdot hr^{-1}$$

The total short-lived ($\tau_{\frac{1}{2}} \leq 15$ hr) saturation activity is therefore (r = 1m):

$$\boxed{\dot{X}_s(Cu + Al) = (28 + 10) \ Rhr^{-1} = 38 \ Rhr^{-1}} \qquad (3.9)$$

The contributions from two important sources to the total activity are not yet included in (3.9), since their $\tau_{\frac{1}{2}}$-values makes them special cases. For this reason they will be treated seperately:

Activity due to ^{62}Cu

The residual activity from ^{62}Cu, produced via the reaction

$$^{63}Cu(\gamma,n)^{62}Cu$$

is a special case, since the half-life time is very short: $\tau_{\frac{1}{2}}$ = 9.78 m. This means that the original (saturation) activity (t=0) after 1 hour has been reduced already by a factor $e^{\frac{-0.69 * 60}{9.78}} = 1.45_{10}{-2}$
The saturation activity, however, is not small:

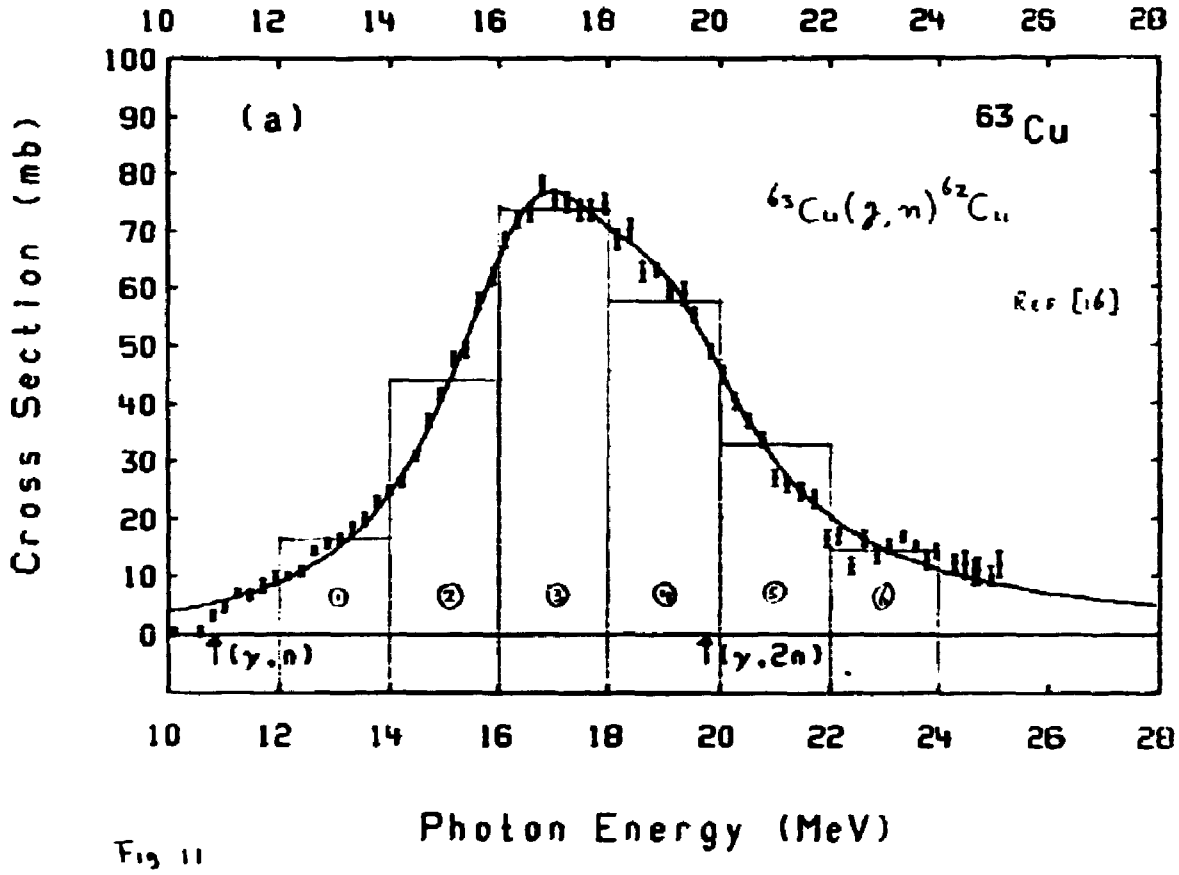

Fig 11

Evaluation of $\sum_{1}^{6}[(\sigma/\bar{E}^2)\Delta E]$ yields σ_{-2}; we find

$$\sigma_{-2}(^{63}\mathrm{Cu}(\gamma,n)^{62}\mathrm{Cu}) \sim 1.64 \text{ mb.MeV}^{-1} \qquad (3.9A)$$

From (19), p+317-323, we obtain: $\Gamma = 0.508$ (R.hr^{-1}m^{-2}/curie). (3.9B)

Substitution Of (3.9A) and (3.9B) into (3.1) yields (r = 1m):

$\chi_s(^{62}\mathrm{Cu}) = 5.8_{10}{-2} * 7 * \frac{13}{62} * 1640 * 0.508 = 71$ Rhr^{-1}

Activity, 1 hour after beam shut-off: $1.45_{10}{-2} * 71 = 1$ Rhr^{-1}

after 2 hours: $(1.45_{10}{-2})^2 = 2.1_{10}{-4}$, so

Activity, 2 hours after beam shut-off: $2.1_{10}{-4} * 71 = 15$ mR hr^{-1}.

Activity due to ^{22}Na.

^{22}Na has a $\tau_{\frac{1}{2}}$-value of 2.62y. Due to the large value of $\tau_{\frac{1}{2}}$, the saturation activity (i.e. the equilibrium between generation and decay) will not be reached in the expected life span of the beam absorber. The activation level due to ^{22}Na therefore will be much lower than $\dot{X}_s$, but slowly rising as time passes by (depending on the integrated product [dissipated power * time]). In order to evaluate X_t, we first calculate X_s in the usual way:
$\sigma_{-2}(^{22}Na) \sim 4.7$ μb.MeV^{-1} ; $\Gamma \sim 1.20$ (17)

$$\xrightarrow{(3.1)} \dot{X}_s = 5.8_{10}{-2} * 90 * \frac{23.3}{27} * 4.7 * 1.2 = 25 \text{ R.hr}^{-1}$$

The expression for X_t is given by (17):

$$X_t = \dot{X}_s \left[\frac{\ell n 2}{\tau_{\frac{1}{2}}} \int_{-\infty}^{0} P(t') e^{\frac{t' \ell n 2}{\tau_{\frac{1}{2}}}} dt' \right] e^{-\frac{t \ell n 2}{\tau_{\frac{1}{2}}}} \qquad (3.10)$$

The term inside the brackets describes the dose build-up till t = 0; the last term describes the exponential decay.
Since $t << \tau_{\frac{1}{2}}$ we may replace both exponentials by unity; this means $X_t \neq f(t)$ any more (as we qualitatively argued already).
Since the irradiation time of the absorber is T, rather than infinity, (3.10) turns over in

$$X_T = \dot{X}_s \frac{\ell n 2}{\tau_{\frac{1}{2}}} \int_{-T}^{0} P(t') dt' \qquad (3.11)$$

By replacing the integral by a sum, and plugging in the relevant numbers, we finally get

$$X_T[\text{R.hr}^{-1}] = 25 \frac{0.69}{2.62 * 365} \sum \left\{ P_{Al}[30\text{kW}] \cdot T[\text{days}] \right\} \quad , \text{ or}$$

$$X_T[\text{R.hr}^{-1}] = 2.4_{10}{-4} \sum \left\{ P_{Al}[\text{kW}] \cdot T[\text{days}] \right\} \qquad (3.12)$$

example: T = 12 days; P_{tot} = 100 kW (i.e. $P_{Al} \sim 90$ kW)

χ = 0.22 Rhr^{-1}

T = 56 days; P_{tot} = 100 kW

χ = 1.0 Rhr^{-1}

Summarizing the previous results:

^{24}Na ($\tau_{\frac{1}{2}}$ = 15 hr): 28 Rhr^{-1}

^{61}Cu ($\tau_{\frac{1}{2}}$ = 3.3 hr): 4 Rhr^{-1}

^{64}Cu ($\tau_{\frac{1}{2}}$ = 12.7 hr): 6 Rhr^{-1}

We define an "effective $\tau_{\frac{1}{2}}$" according to

$$\tau_{\frac{1}{2}}^{eff} \equiv \frac{\sum \tau_{\frac{1}{2}} \cdot \dot{\chi}_s}{\sum \dot{\chi}_s} \Rightarrow \tau_{\frac{1}{2}}^{eff} \sim 13.5 \text{ hr}$$

Putting everything together, we get:

$$\dot{\chi}\,[Rhr^{-1}] = 0.38\, P_{tot}[kW]\, e^{-\frac{t[hr]\ln 2}{13.5}} + 1.8_{10}{-4} \sum \left\{ P_{tot}[kW] \cdot T[\text{days}] \right\} \qquad (3.13)$$

t is time after beam shut-off

T is irradiation time

$\dot{\chi}$ is given for a <u>distance of 1 meter</u>

The behaviour of $\dot{\chi}$, as a function of time, is given on the next two pages.

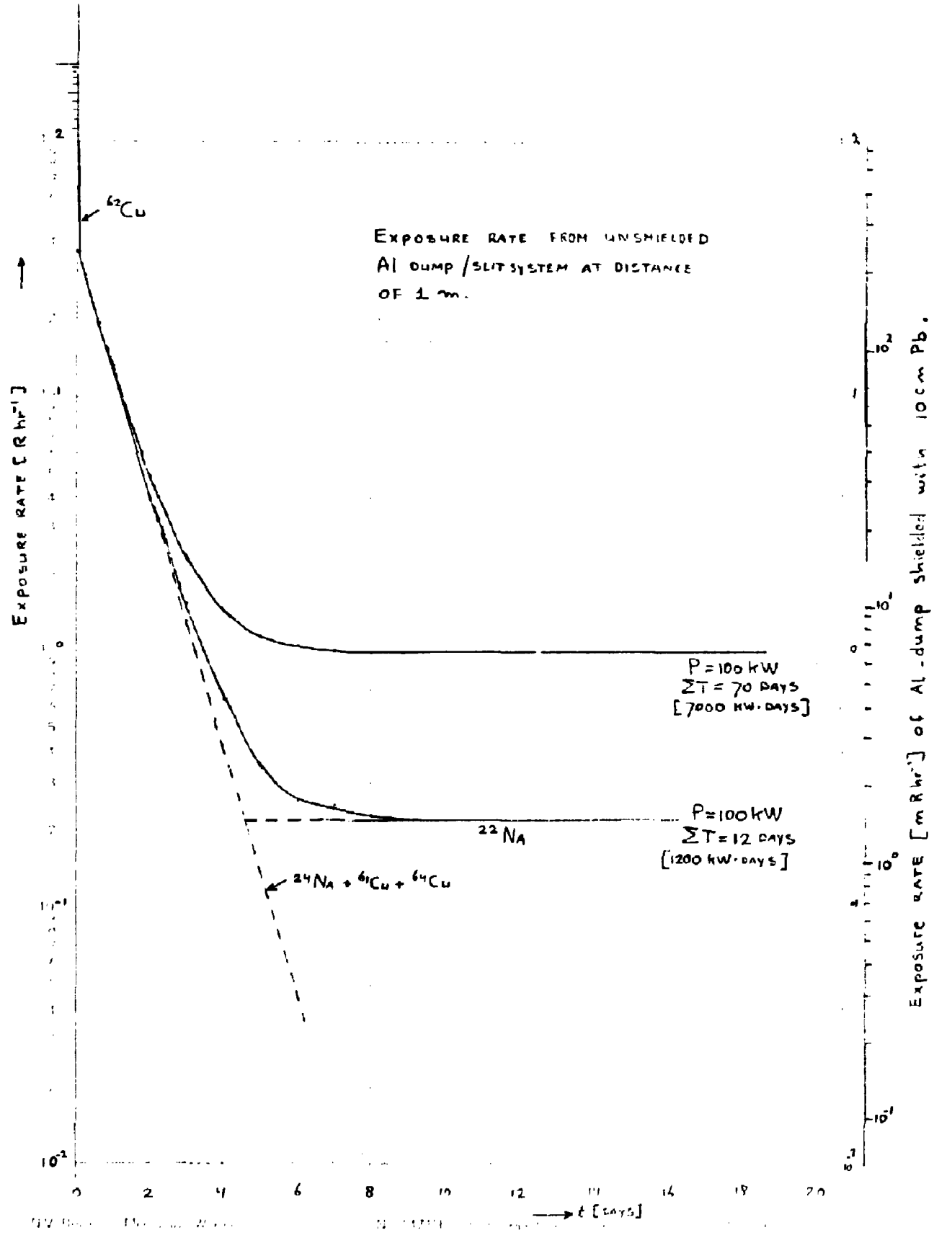
EXPOSURE RATE FROM UNSHIELDED Al DUMP / SLIT SYSTEM AT DISTANCE OF 1 m.
^{62}Cu
P = 100 kW
ΣT = 70 DAYS
[7000 KW·DAYS]
P = 100 kW
ΣT = 12 DAYS
[1200 KW·DAYS]
^{22}Na
$^{24}Na + ^{61}Cu + ^{64}Cu$
EXPOSURE RATE [R hr^{-1}]
EXPOSURE RATE [m R hr^{-1}] of Al-dump shielded with 10 cm Pb.
t [DAYS]

Fig 12

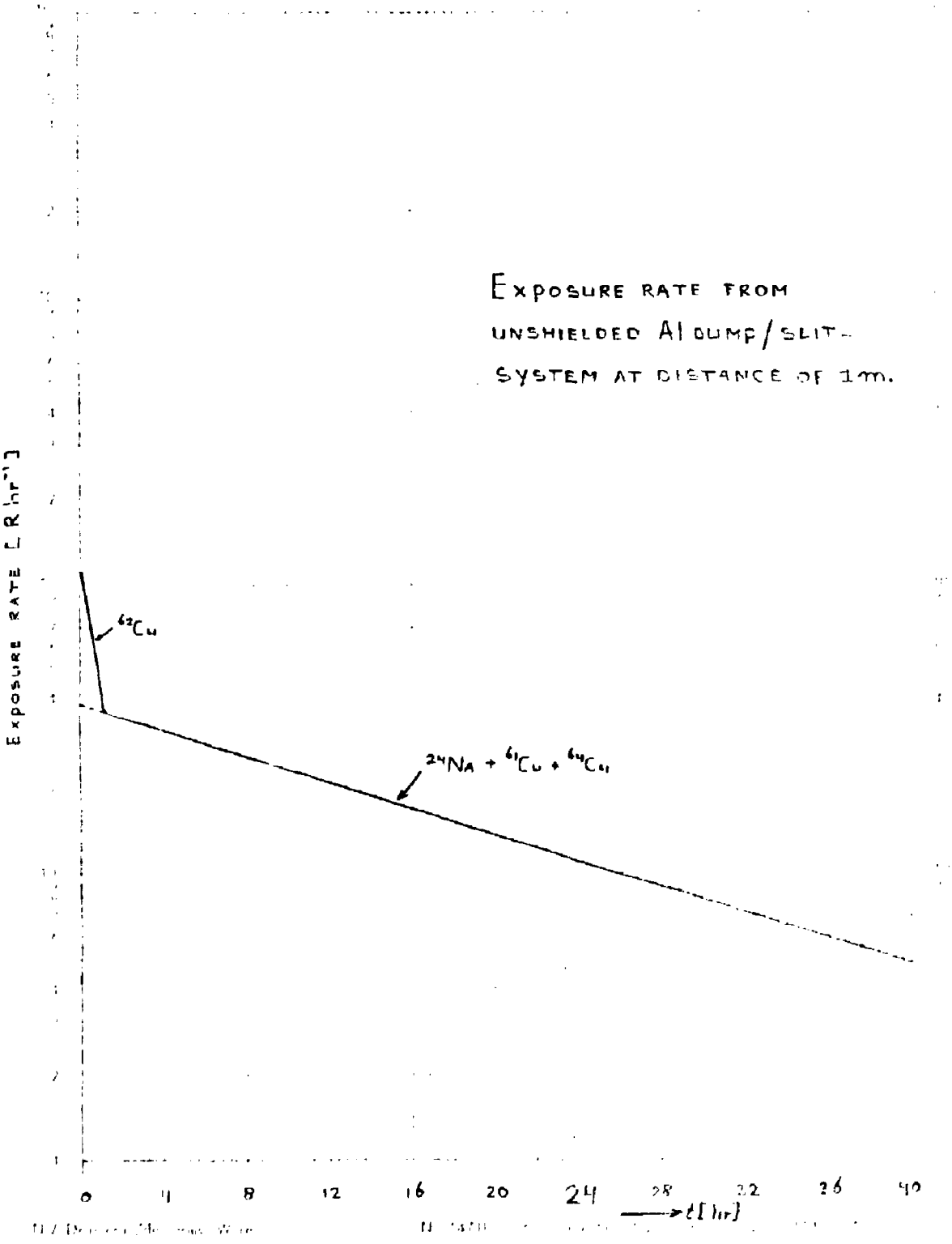
Exposure rate from
unshielded Al dump/slit-
system at distance of 1m.
Exposure rate [R hr⁻¹]
⁶²Cu
²⁴Na + ⁶¹Cu + ⁶⁴Cu
0
4
8
12
16
20
24
28
32
36
40
t [hr]

Fig 13

4. Radiation from copper collimators.

The beam handling system is protected at various places by copper collimators. The dimensions of those collimators depend on the beam size at some particular location. Generally speaking, however, they all look something like:

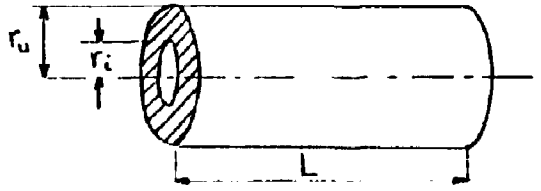

$(r_u - r_i) \sim 4$ à 5 cm
$L \sim 20$ cm

Fig. 14

The maximum incident power is $\sim$ 10 kW (the Y-collimator after the slits has a higher power rating: $\sim$20 kW).
In order to estimate the radiation level from the collimators, we follow the same approach as in the case of the slit-dump system; we first consider the beam-on situation; the residual-activity problem is treated next.

Gamma's.

The angular distribution of the gamma intensity is given in Fig. 15 (a figure we borrowed from an inter-departmental note of W. Turchinetz from MIT: "Radiation Doses in Vicinity of the Spectrometer Target Chamber"). A similar figure is presented in ref (1), p. 1032. The values of the dose rate in the region $\theta \sim 0^0$ should be interpreted with care: from ref. (1) p. 1033, we quote two results: E_0 = 990 MeV, L = 21.4 R.L.: dose rate, $\theta = o^\circ$ $1.1_{10}4$ RAD.hr^{-1}

E_0 = 12 GeV, L = 16 R.L.: dose rate, $\theta = o^\circ$ $1.2_{10}5$ RAD.hr^{-1}

both numbers for 1 kW incident power, at distance of 1 meter. The difference in length is $(21.4-16)\chi_0(Cu) = 5.4 * 1.4$ cm = 7.56 cm; attenuation of gamma's in copper is given by $e^{-0.25t(cm)}$, so in our case $e^{-0.25* 7.56} \sim 0.15$.

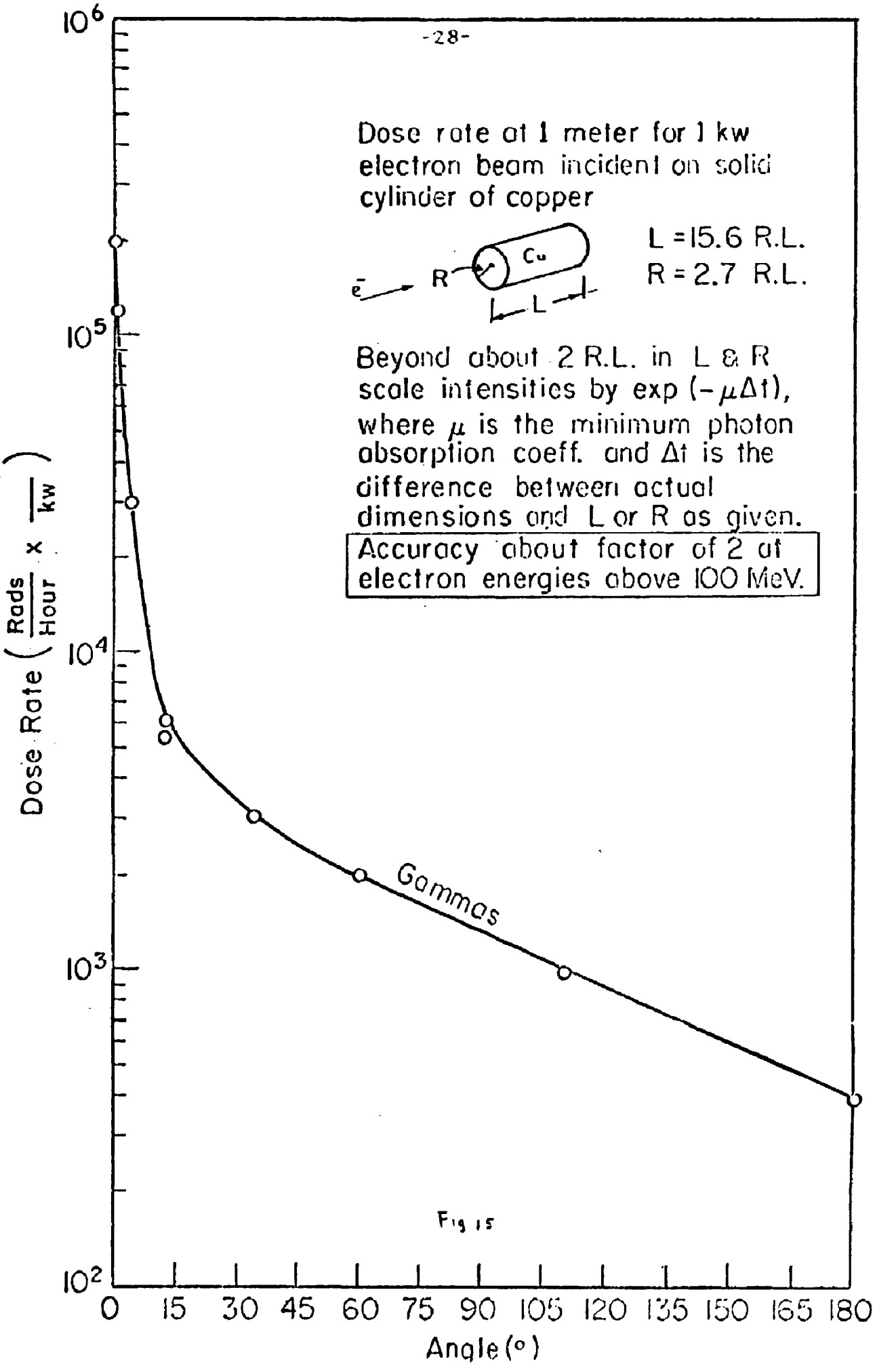
Dose rate at 1 meter for 1 kw electron beam incident on solid cylinder of copper
L = 15.6 R.L.
R = 2.7 R.L.
e⁻
R
Cu
L
Beyond about 2 R.L. in L & R scale intensities by exp (−μΔt), where μ is the minimum photon absorption coeff. and Δt is the difference between actual dimensions and L or R as given.
Accuracy about factor of 2 at electron energies above 100 MeV.
Gammas
Dose Rate (Rads/Hour × 1/kw)
10⁶
10⁵
10⁴
10³
10²
0 15 30 45 60 75 90 105 120 135 150 165 180
Angle (°)

Fig 15

The values for the dose rate, quoted above, therefore are consistent within, say 50%. As indicated already in Fig.15 , one should scale the intensities according to $\exp(-\mu.t)$, $\mu = 0.25\ cm^{-1}$, (t) = cm.

Low-energy neutrons.
As mentioned before, one should regard the dose-equivalent rate for low-energy neutrons as an isotopic contribution to the total amount of radiation emanating from the collimator.
From Table I, we infer:
dose-equiv. rate (at 1m, per kW): $Y_{GR} = 1.2_{10}3\ rem.hr^{-1}$.
(we have taken the average of Approx. A & Approx. B).

High-energy neutrons.
In order to estimate the high-energy neutron yield, Y_H, we lean heavily on the results as given in sect. 2.3. Those results were based on Cu-data, and have been "transformed" to be valid for aluminium. The RBE-factor has also been folded in these results. Rather than repeat all those tedious calculations, we simply take the Al-results and transform them back to Cu according to:

$$Y_H(Cu) = \frac{\chi_o(Cu)}{\chi_o(Al)}\ Y_H(Al) = 0.54\ Y_H(Al) \qquad (4.1)$$

The value of $Y_H(Al)$ is given in Fig. 7 (we take the case $\theta = 90^0$ only): $Y_H(Al) = 1.8_{10}2\ rem.hr^{-1}$ (r = 1m, per kW incident power) so, from (4.1), we get $Y_H(Cu) \sim 100\ rem.hr^{-1}$ (" , $\theta = 90^0$).

Residual activity.
In order to estimate the residual activity from the slit system we assumed that 10% of the incident power is absorbed in the copper module. Since the power rating of most of the collimators is ~10 kW, it seems reasonable to assume that the resodual activity of a copper collimator (10 kW incident power) is equal to the residual activity from the copper part of the slit system (at 100 kW incident power):

$\dot{X}_s(^{61}Cu) = 4\ R.hr^{-1}$ ($\tau_{\frac{1}{2}} = 3.3$ hr)
$\dot{X}_s(^{64}Cu) = 6\ R.hr^{-1}$ ($\tau_{\frac{1}{2}} = 12.8$ hr)
$\dot{X}_s(^{62}Cu) = 71\ R.hr^{-1}$ ($\tau_{\frac{1}{2}} = 0.2$ hr)

at distance of 1 m
incident power 10 kW

Two hours after beam shutt-off, the contribution from ^{62}Cu has become already negligably small ($\sim$15 $mR.hr^{-1}$). The contribution from ^{61}Cu has been reduced to $\sim$0.3 $R.hr^{-1}$ after T = 12 hr. So, for $T \gtrsim 12$ hr, the residual activity from the collimator is given by:

$$X_T[Rhr^{-1}] \sim 6\, e^{-\frac{0.69\,T[hr]}{12.8}} \qquad (4.2)$$

We want to make two final remarks:

1. If we assume that the collimator consists of a pure ^{65}Cu, ^{63}Cu mixture, we do not expect, as in the case of Al, any substantial contribution from a long-lived isotope. It is true that the reaction $^{63,65}Cu$ (γ, something) makes much more than only $^{61,62,64}Cu$; e.g. the cobalt isotopes are rather long-lived. Their yield however (e.g. compared to that of ^{62}Cu) is so small, that within the life-expextancy of a collimator the activity of those components will not reach a dangerous level. Table II (from ref. (1)) list some daughters produced by γ's on copper:

DAUGHTER	$\tau_{\frac{1}{2}}$(hr)	E_γ (MeV)	YIELD REL. TO ^{62}Cu
^{57}Ni	36	1.4, 1.9	$1.8_{10}{}^{-3}$
^{60}Co	$6.6_{10}{}^{4}$	1.17,1.33	$2_{10}{}^{-2}$
^{58}Co	$2.5_{10}{}^{3}$	0.80	$2.7_{10}{}^{-2}$
^{56}Co	$2.7_{10}{}^{3}$	0.89	$1.2_{10}{}^{-2}$
^{55}Co	26	many	$8.5_{10}{}^{-4}$
^{59}Fe	$1.6_{10}{}^{3}$	1.1, 1.3	$3_{10}{}^{-3}$
^{56}Mn	3.7	0.8, 2.8	$3_{10}{}^{-3}$
^{54}Mn	$1_{10}{}^{4}$	0.8	$5_{10}{}^{-3}$
^{52}Mn	$2_{10}{}^{2}$	1.4	$1.3_{10}{}^{-3}$

Table II. Gamma-induced activities in copper.

2. Although the (watercooled) collimators are rated at 10 kW, it is very unlikely (and certainly very undesirable) that this amount of beam power will be dissipated during a prolongued period of time at a collimator. An expected beam loss of ∿1 kW per collimator seems a much more reasonable estimate (except maybe for the Y-collimator directly behind the slits). A reasonable estimate of the residual activity therefore is (cf.eq.(4.2) :

$$\dot{X}_T\,[R.hr^{-1}] \sim 0.6\, e^{-\frac{0.69\,T[hr]}{12.8}} \quad , \; T \gtrsim 12\ hr \qquad (4.3)$$

$$T = 0 \Rightarrow 600\ mR.hr^{-1} \begin{cases} 5\ cm\ Pb \rightarrow \text{factor } 8.2_{10}{}^{-2} \rightarrow 50\ mR.hr^{-1} \\ 10\ cm\ Pb \rightarrow \text{factor } 6.7_{10}{}^{-3} \rightarrow 4\ mR.hr^{-1} \end{cases}$$

5. Shielding

In almost all cases lead is the most suitable material to attenuate the radiation dose due to gamma radiation. Lead shielding is very effective in that respect as becomes clear from table III: every 5 cm of lead reduces the radiation level more than a factor 10. We propose to place lead shielding of at least 10 cm thickness all around the vacuum tank of the slits. The principal function of the lead shield will be to provide personnel protection during beam-off periods. The reduction factor for 10 cm lead is $7_{10}{}^{-2}$. Fig. 12 gives the (residual) radiation level at r = 1m from the unshielded slit-system. From this we calculate the residual radiation level for the 10cm lead-shielded slit-system: at time t = 0 the radiation level is 700 mR hr^{-1}, after one hour the radiation level is 250 mR hr^{-1}, after one day we find 90 mR hr^{-1} and after one week the level is 7 mR hr^{-1} after irradiation of 7000 kW days and 1.5 mR hr^{-1} after irradiation of 1200 kW days respectively. Note that the outer right-hand ordinate of Fig. 12 gives the radiation level of the shielded slit-system.

The radiation levels in the vicinity of the slits when the (full 100 kW) beam is on, are indicated in a schematic drawing of the slit-area shown in Fig. 17. We see that, while the gamma radiation constitutes the major contribution to the total radiation before the shielding, after the shielding the neutron dose contributes most in all cases.

The philosophy for neutron shielding is first to slow-down the neutrons and subsequently to remove them by capture reactions. A cheap and good material for this purpose is concrete. The attenuation for neutrons of concrete (TSF-5.5 (22), ρ = 2.32 gcm^{-3}) is given as a function of thickness of the shield in Fig. 16. The dose-equivalent rate due to low-energy (GR) neutrons is attenuated much more by concrete shielding than the dose-equivalent rate due to high-energy neutrons. We used transmission curves for mono-energetic neutrons given in appendix F of ref. (22). The low-energy neutrons (E_n < 15 MeV) have a few MeV average energy. The transmission curves do not vary substantially in the energy range from 2 to 14 MeV. We took the transmission curve for 2.7 MeV for the calculation of the attenuation factor of the low-energy neutrons in concrete.
Lead hardly attenuates the low-energy neutron dose rate, as was measured at SLAC (24) and shown in Fig. 18b. Therefore, we took an attenuation factor unity in this case.

For the calculation of the attenuation factor of the high-energy neutrons we need to know the energy spectrum. The energy spectrum of the high-energy neutrons was taken from Monte-Carlo calculations by Gabriel and Alsmiller (13), who computed neutron yields from 400 MeV electrons incident in a thick copper target: the energy spectrum at emission angles between 0 and 30 degrees is shown in Fig. 6b. In order to calculate the attenuation factor A for high-energy neutrons in concrete, we will follow a similar procedure as performed in the calculation of the total neutron dose rate (eq. 2.9). Namely:

$$A(d) = \sum_i \alpha_{E_i}(d) \left(\frac{d^2n}{dE\,d\Omega}\right)_{E_i} \Delta E_i \Big/ \sum_i \left(\frac{d^2n}{dE\,d\Omega}\right)_{E_i} \Delta E_i \qquad (5.1)$$

where α_{E_i} (d) represents the attenuation factor for mono-energetic neutrons with energy E_i after thickness d. The α_{E_i} values are calculated directly from appendix F of ref. (22). For large values of d (d > 1m) the mean free path of the neutrons can be described with $\lambda \sim 105$ gcm^{-2}. This gives an attenuation which is proportional to exp(-0.022 * d(cm)), corresponding to eq. 2.6. (see also (9)). The curve given in Fig. 16 represents the attenuation factor for neutrons emitted in forward direction (0-30 degr.). The radiation field around the slits as indicated in Fig. 17 is now further evaluated using the data given in Fig. 16. The attenuation in lead of high-energy neutrons was calculated using a mean free path of $\lambda_{Pb} \sim 280$ gcm^{-2} (1), giving $A = e^{-0.042 * d\ (cm)}$ (see table III). This is a crude approximation, but the effect is small anyway.

The neutron dose rate is attenuated only in forward direction as indicated in the schematical drawing of Fig. 17. Especially the low-energy neutron fluxes, which are isotropic, still give a large contribution ($6_{10}4$ rem hr^{-1} at r = 1m). The low-energy neutron dose equivalent rate, however, can easily be attenuated with polyethylene, placed after the lead shielding. The dose equivalent transmission of 30cm polyethylene is $1._{10}$-2 (24), see Fig. 18a.

We propose to place polyethylene blocks of at least 20cm thickness around the lead shielding, followed by thin boron-loaded polyethylene sheets. In that case the neutrons emitted from the slit-modules are slowed-down in the lead, further slowed down and attenuated in the polyethylene and removed by capture reactions in the boron-loaded polyethylene sheets.

With the shielding as proposed above, we believe that the total radiation everywhere outside the shielding can be maintained below 10^4 rem hr^{-1} when the full (100 kW) beam is dumped in the slit modules.

Table III: Attenuation coefficients for γ's, L- and H neutrons of Pb, Cu and concrete (rules of thumb)

	CONCRETE $e^{-0.05d(cm)}$	LEAD $e^{-0.5d(cm)}$	COPPER $e^{-0.25d(cm)}$
Gamma's	example: d = 50 cm $e^{-0.05*50}=e^{-2.5}=8.2_{10}-2$	example: d = 10 cm $e^{-0.5*10}=e^{-5}=6.7_{10}-3$	example: d = 25 cm $e^{-0.25*25}=e^{-6.25}=1.9_{10}-3$
Low-energetic neutrons	E_n = 2.7 MeV 50 cm → $3.9_{10}-2$ 100cm → $3.9_{10}-4$ 150cm → $7_{10}-6$ See also Fig 16	$E_n \sim$ 2 MeV $\sim$1	$E_n \sim$ 2 MeV $\sim$1
High-energetic neutrons	15 MeV $\lesssim E_n \lesssim$ 400 MeV: $e^{-0.022d(cm)}$, d > 100cm 50 cm → 0.51 each additional 100 cm → 0.15 ↓ 50 cm: factor 150 cm → $5_{10}-2$ 0.33 ------ $(0.33)^2=e^{-2.2}=0.11$ see also Fig. 16	$E_n \gtrsim$ 150 MeV: $e^{-0.042d(cm)}$ example: d = 10 cm $e^{-0.042*10}=e^{-0.42}=0.66$	$E_n \gtrsim$ 150 MeV: $e^{-0.045d(cm)}$ example: d = 25 cm $e^{-0.045*25}=e^{-1.125}=0.33$

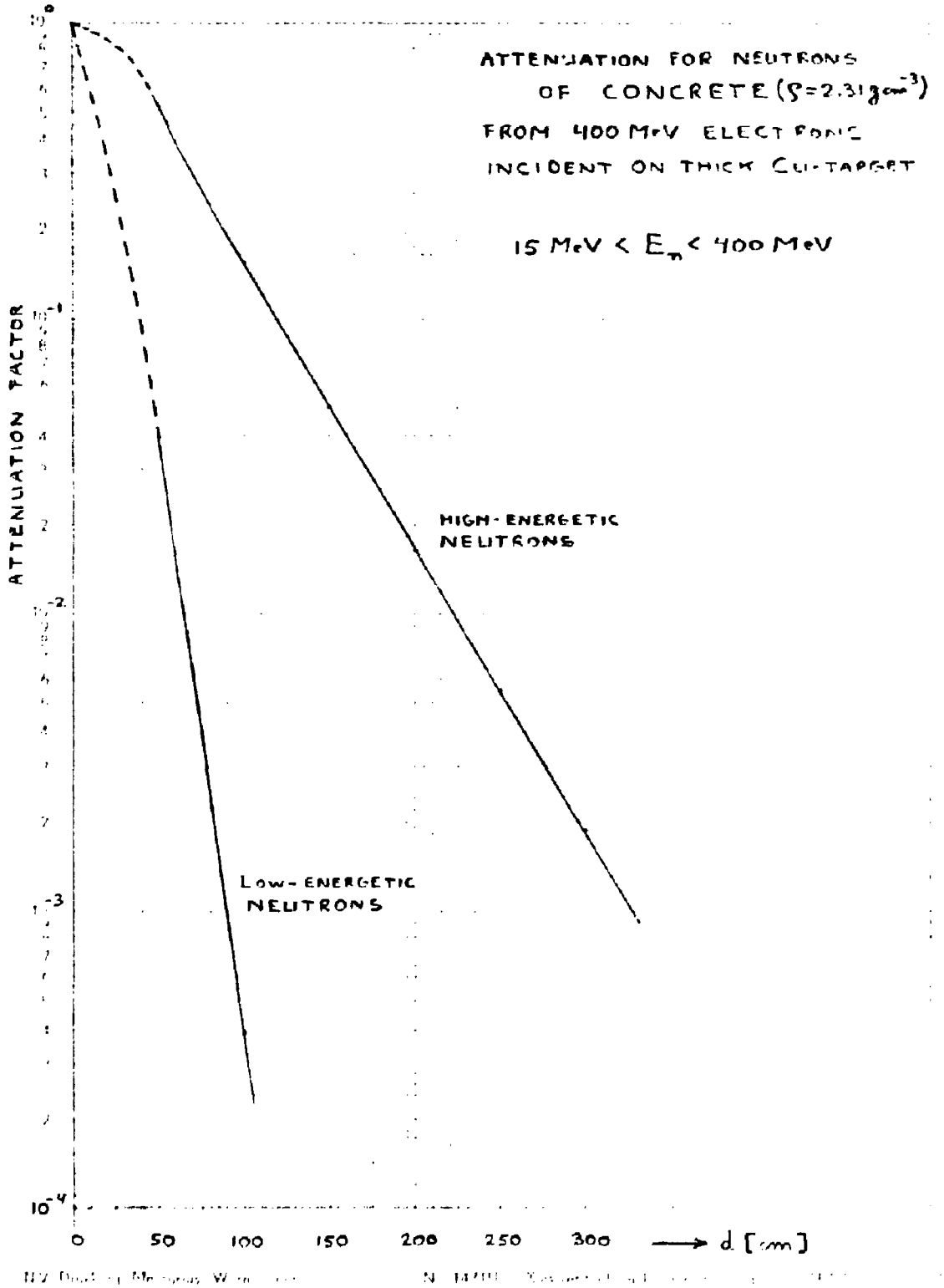
ATTENUATION FACTOR
ATTENUATION FOR NEUTRONS
OF CONCRETE (ρ=2.31 g cm⁻³)
FROM 400 MeV ELECTRONIC
INCIDENT ON THICK Cu-TARGET
15 MeV < E_n < 400 MeV
HIGH-ENERGETIC
NEUTRONS
Low-ENERGETIC
NEUTRONS
10⁻¹
10⁻²
10⁻³
10⁻⁴
0
50
100
150
200
250
300
d [cm]

Fig 16

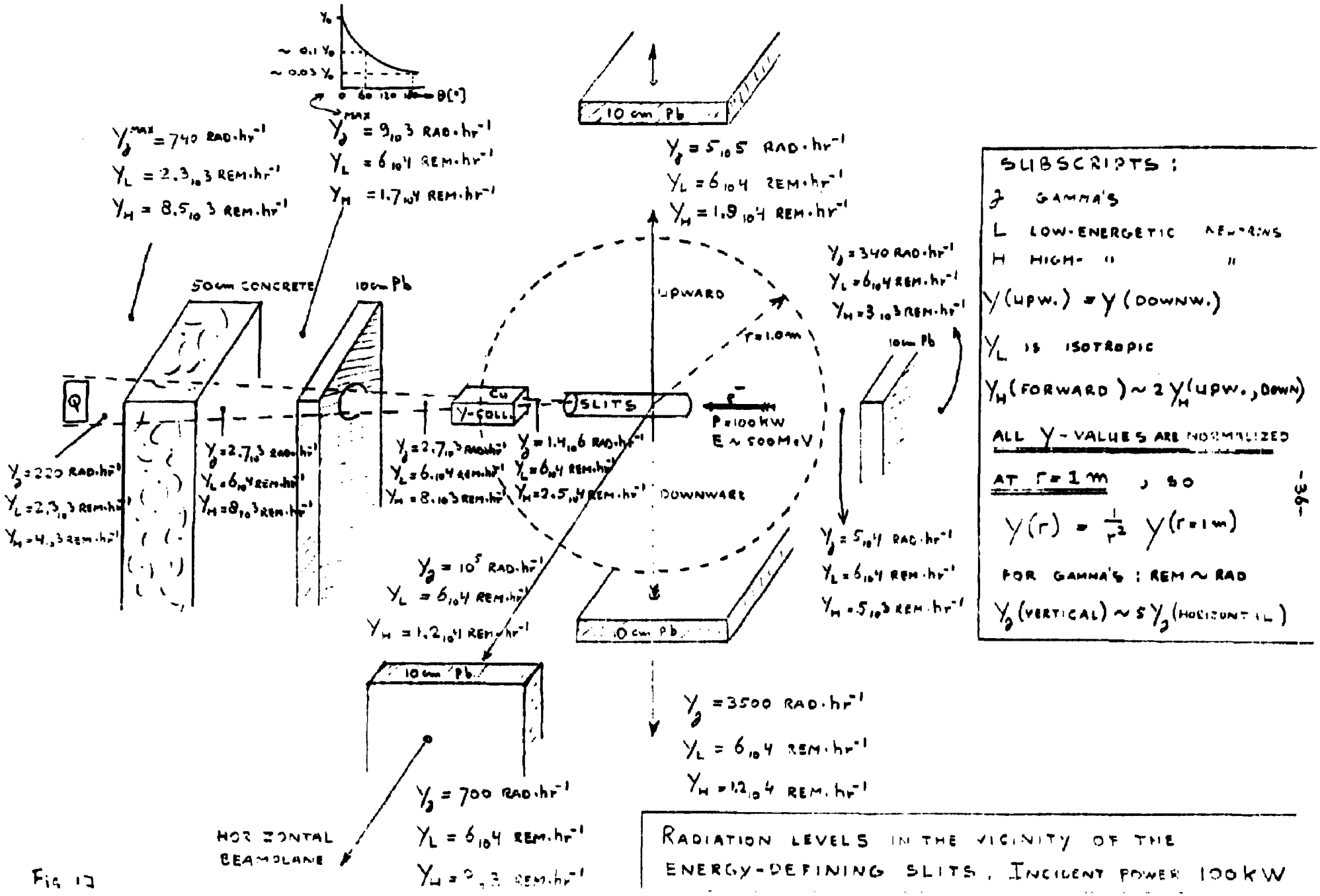

RADIATION LEVELS IN THE VICINITY OF THE ENERGY-DEFINING SLITS, INCIDENT POWER 100 kW

Fig 12

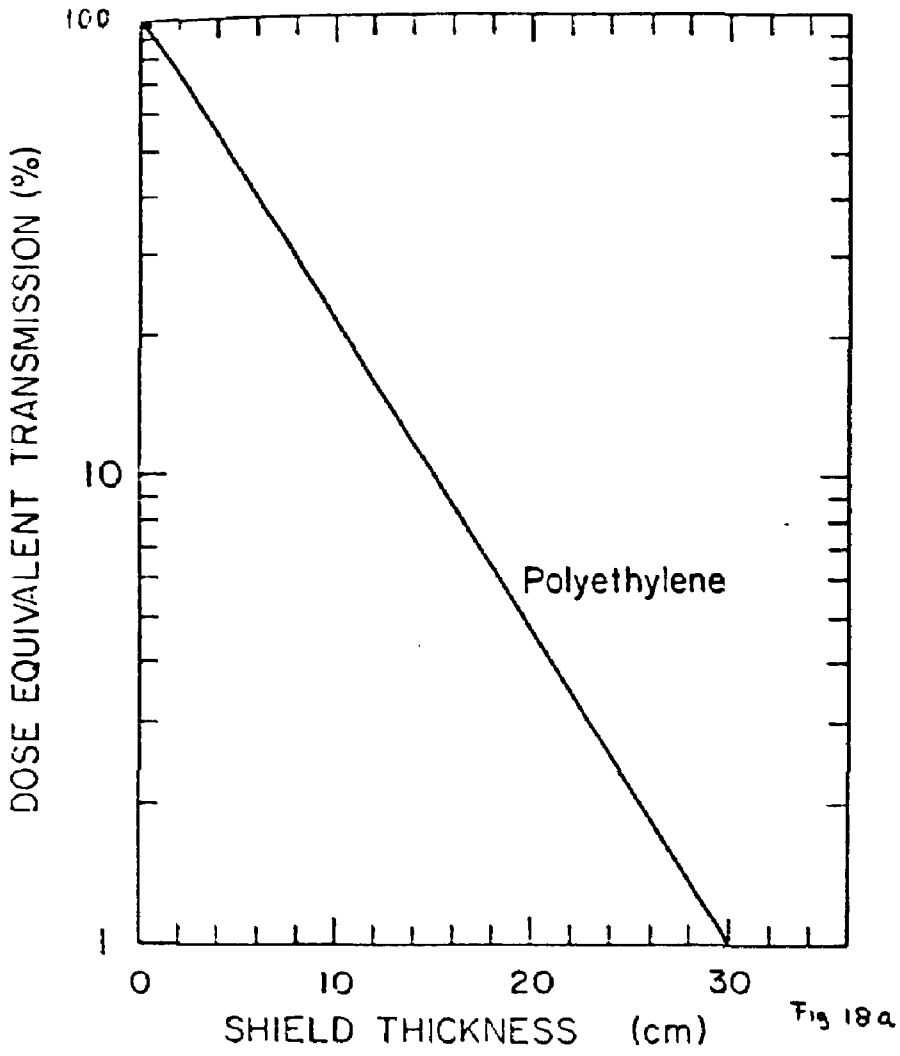

Fig 18a

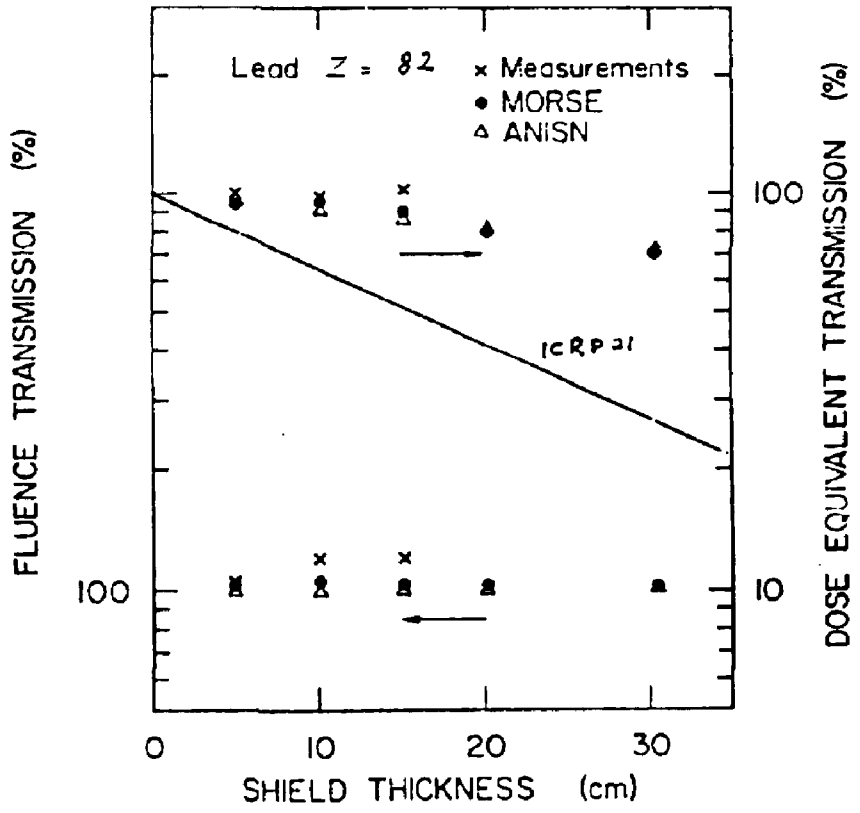

Fig. 18 b

Fig 18 – The dose equivalent transmission and fluence transmission as a function of shield thickness (see for description ref. [24]).

Appendix A

Some useful numbers and relations concerning radiation.

Photon flux (E_γ = 0.2 - 2 MeV)

1 MeV cm^{-2} = 4.6_{10}-10 rem (20); multiplication by (t^{-1}):

1 MeV $cm^{-2}sec^{-1}$ = 1.66_{10}-3 m rem hr^{-1} --------- (A-1)

Further: 1 MeV sec^{-1} = 1.6_{10}-13 W ---------- (A-2)

(A1)+(A2) $\boxed{1\ W\ cm^{-2} \sim 1_{10}10\ m\ rem\ hr^{-1}}$ ---------- (A-3)

1 rad = 100 erg g^{-1}; 1 erg = 1_{10}-7 J

1 rad = 1_{10}-5 J g^{-1} 1 Curie = $3.7_{10}10$ disint. sec^{-1}

$$1\ rad = \frac{2.17_{10}9}{E_\gamma(MeV)}\ photons\ cm^{-2}, \quad E_\gamma = 0.07 - 2.0\ MeV \quad (23)$$

Neutrons rem = rad * RBE---------- (A-4)

RBE is Relative Biological Effectiveness

E_n (MeV)	RBE	
thermal	3	Ref (20)
1_{10}-4	2	
5_{10}-3	2.5	
0.1	5	→ Giant Resonance neutrons: RBE ∿ 7
10	6.5	

Fig. A1 presents a graphical representation of these data.

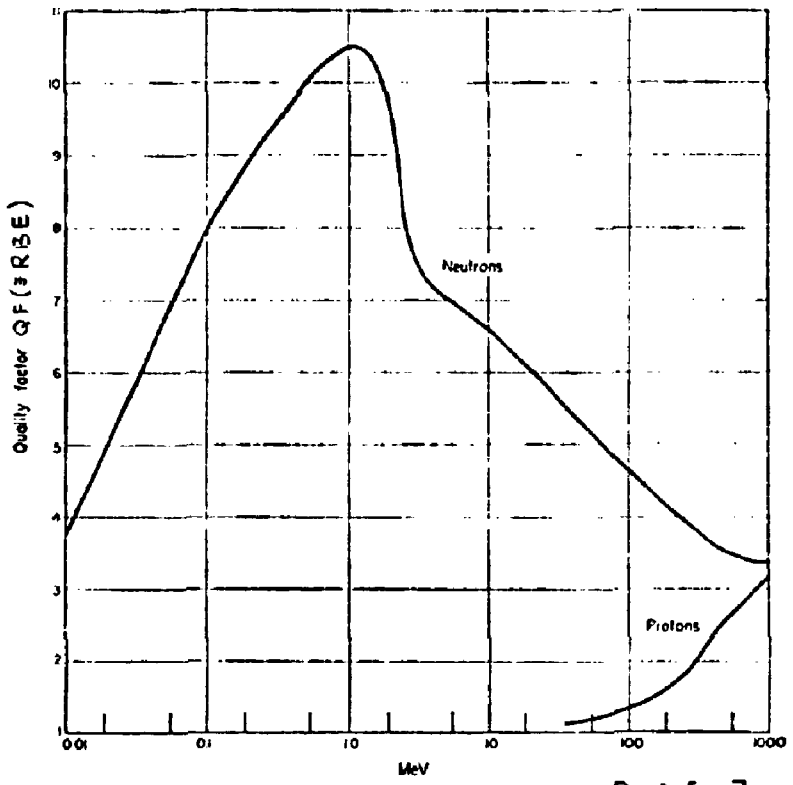

Fig A1 Values of *QF* for neutrons and protons of various energies. REF [21]

In order to convert neutron flux into dose-equivalent rate one should know the, energy dependent, conversion factor. Fig. A2 and Table A1 provide information about this factor.

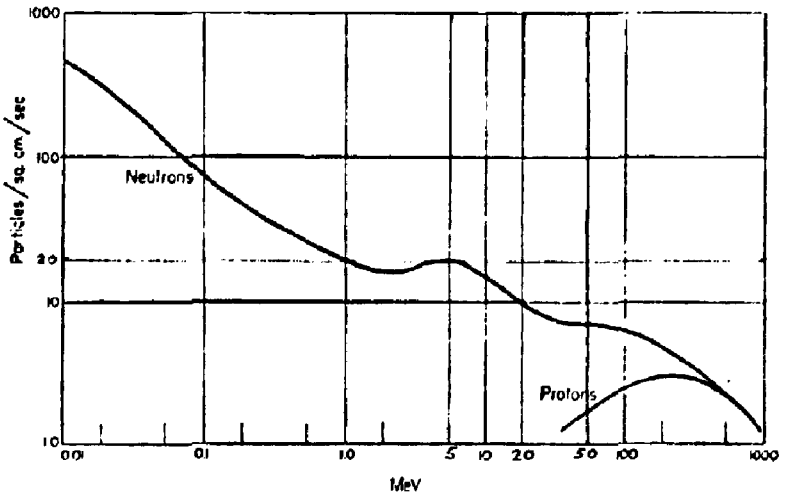

FIG. A2 Particle flux densities corresponding to a dose rate of 2.5 mrem/h. The flux values are for primary particles in beams assumed to be in equilibrium with secondary particles as a result of passage through shielding. The curves are smoothed from tabulated data by Snyder[3] and Neary and Merwin[4].

REF [21]

B.3 Mean Quality Factors, $\bar{Q}$,[a] and Fluence Rates per Unit Dose-Equivalent Rate for Monoenergetic Neutrons[b] REF [22]

Neutron energy MeV	$\bar{Q}$ (≡ RBE)	Fluence rate per unit dose-equivalent rate cm^{-2} s^{-1}/mrem h^{-1}	mrem h^{-1} PER n cm^{-2} s^{-1}	— SAME, REF [21] Tab A2
2.5×10^{-8} (thermal)	2	270		
1×10^{-7}	2	270		
1×10^{-6}	2	220		
1×10^{-5}	2	220		
1×10^{-4}	2	230		
1×10^{-3}	2	270		
1×10^{-2}	2.5	280		
1×10^{-1}	7.5	46	0.02	
5×10^{-1}	11	11	0.09	
1	11	7.6	0.13	0.13
2.5	9	8.0	0.13	
5	8	6.4	0.16	0.13
7	7	6.8	0.15	
10	6.5	6.8	0.15	0.17
14	7.5	4.8	0.20	
20	8	4.4	0.23	0.25
40	7	4.0	0.25	50 MeV 0.36
60	5.5	4.4	0.23	
100	4	5.6	0.18	0.40

[a] Value of quality factor at the point where the dose equivalent is maximum in a 30-cm tissue-equivalent phantom.

[b] Monoenergetic neutrons incident normally on a 30-cm-thick tissue-equivalent phantom.

TABLE A1

From Table A1 we infer that in the region $E_n \sim$ 1-20 MeV the data from refs. (21) and (22) are in fair agreement. For $E_n \geq 40$ MeV however, there exists a fairly large discrepancy. Since the data from ref. (22) are more recent, we adopt the values as given in the 4th column of Table A1.

Slow neutrons (E_n = 1-10 MeV): 0.14 $\frac{\text{m rem hr}^{-1}}{\text{n cm}^{-2}\text{sec}^{-1}}$

Fast neutrons ($E_n \geq$ 10 MeV): 0.30 $\frac{\text{m rem hr}^{-1}}{\text{n cm}^{-2}\text{sec}^{-1}}$

The data from ref. (21) are also used in ref. (10), see Fig. A3.

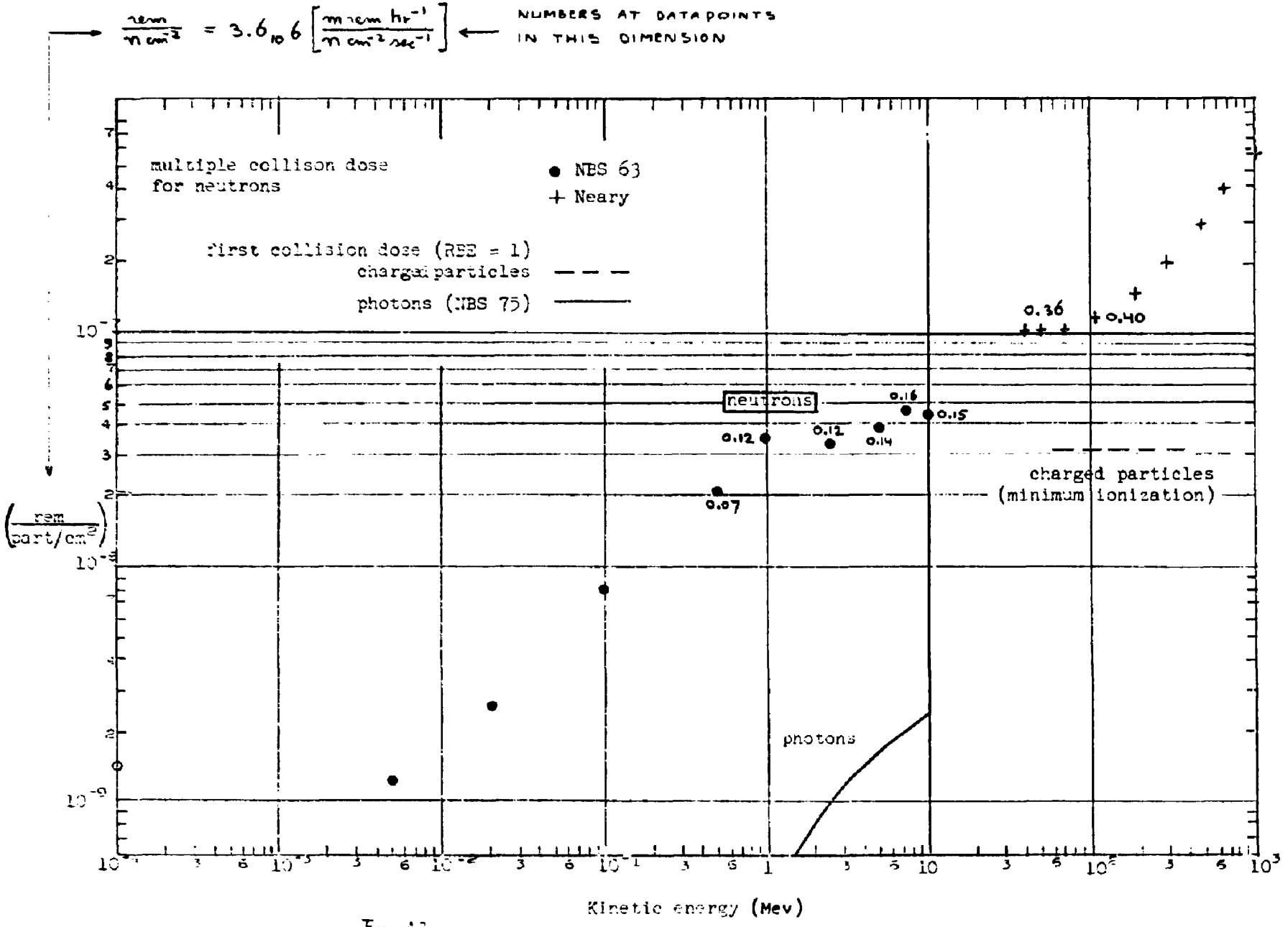
$\frac{rem}{n\,cm^{-2}} = 3.6_{10}6 \left[\frac{m\,rem\,hr^{-1}}{n\,cm^{-2}\,sec^{-1}}\right]$
NUMBERS AT DATA POINTS IN THIS DIMENSION
multiple collison dose for neutrons
● NBS 63
+ Neary
first collision dose (REE = 1)
charged particles
photons (NBS 75)
0.36
0.40
neutrons
0.16
0.15
0.12
0.12
0.14
0.07
charged particles
(minimum ionization)
photons
$\left(\frac{rem}{part/cm^2}\right)$
Kinetic energy (Mev)

Fig A3

The conversion from $n.cm^{-2}$ *to rad (2nd part of Table A2) proceeds as follows:*

fast neutrons: $0.3 \frac{\text{m rem hr}^{-1}}{\text{n cm}^{-2}\text{sec}^{-1}} = 0.3 \frac{1_{10}{}^{-3}\text{ rem}}{3600\text{ n cm}^{-2}} = 8.33_{10}{}^{-8} \frac{\text{rem}}{\text{n cm}^{-2}}$

RBE $\sim$ 6 $\Rightarrow$ conversion factor $1.4_{10}{}^{-8} \frac{\text{rad}}{\text{n cm}^{-2}}$

rem = rad $\times$ RBE.

TABLE A2

B.4 Thresholds for Radiation Damage to Selected Materials and Systems[a] REF [22]

Material	X-Ray and Electron Absorbed Dose
	rads
Transistor	1×10^{3}-2×10^{4}
Potentiometer	1×10^{3}-1×10^{9}
Resistor	5×10^{3}-1×10^{9}
Diode	1×10^{4}-3×10^{4}
Microcircuit	1×10^{4}-1×10^{5}
Glass changes color	1×10^{5}-4×10^{5}
Plastics lose tensile strength	1×10^{6}-1×10^{9}
Natural rubber loses elasticity	5×10^{6}-3×10^{7}
Polymers and oils unusable	1×10^{10}-3×10^{10}
Disinfestation	10^{4}-10^{5}
Pasteurization	10^{5}-10^{6}
Sterilization	10^{6}-10^{7}

	Fast Neutron Fluence	
	$n \cdot cm^{-2}$	RADS
Semiconductor devices		
silicon transistors	1×10^{12}-3×10^{14}	$1.4 \times 10^{4} - 4.2 \times 10^{6}$
diodes	1×10^{12}-3×10^{14}	" "
tunnel diodes	1×10^{14}-1×10^{15}	$1.4 \times 10^{6} - 1.4 \times 10^{7}$
germanium transistors	1×10^{13}-1×10^{15}	$1.4 \times 10^{5} - 1.4 \times 10^{7}$
silicon-carbide diodes	1×10^{15}-1×10^{16}	$1.4 \times 10^{7} - 1.4 \times 10^{8}$
Carbon potentiometers	1×10^{13}-1×10^{16}	
Capacitors		
boron, electrolytic	1×10^{12}-1×10^{14}	
aluminum, electrolytic	1×10^{13}-1×10^{14}	
tantalum, electrolytic	1×10^{15}-1×10^{16}	
paper, oil	1×10^{15}-1×10^{16}	
Vacuum tubes		
gas-filled	1×10^{15}-1×10^{16}	
power	1×10^{15}-1×10^{16}	
photomultiplier	1×10^{15}-1×10^{16}	
Insulators, electrical		
Teflon	1×10^{16}-1×10^{17}	
Bakelite	1×10^{17}-1×10^{18}	
Nylon	1×10^{16}-1×10^{17}	

Material	Neutron Fluence
	cm^{-2}
Crystals	
Rochelle salts	1×10^{17}-1×10^{19}
barium titanate	1×10^{17}-1×10^{19}

[a] Bolt and Carroll (1963); DASA (1969); DNA (1972); Kircher and Bowman (1964); Kohl *et al.* (1961).

Tables A3 and A4 (taken from "Electronics"/March 16, 1978, p131-133) provide information about some specific electronic components. The results are in agreement with the data fromTable A2.
The "Electronics" data were calculated/measured for neutron energies of 1 MeV; from Table A1 $\Rightarrow$ 0.13 m rem hr^{-1} per n cm^{-2} sec^{-1}.

$$\Longrightarrow \quad 1 \text{ n cm}^{-2} = \frac{0.13}{3600} \text{ m rem} = 3.6_{10}\text{-}8 \text{ rem}$$

RBE = 11, so 1 n cm^{-2} = 3.3_{10}-9 RAD

Example: TTL-Logic: 10^{14} n cm^{-2} $3.6_{10}6$ rem $\rightarrow$ $3.3_{10}5$ RAD
we note that the number quoted in Table A3 is $1_{10}6$ RAD (Si), RAD (Si) stands for Rö absorbed dose in silicon. A possible explanation for this "discrepancy" is that RBE and RBE (Si) differ somewhat.

TABLE A3

Radiation environment \ Semiconductor technology		Discrete bipolar transistors and J-FETs	Silicon controlled rectifiers	TTL	Low-power Schottky TTL	Analog integrated circuits	C-MOS	n-MOS	Light-emitting diodes	Isoplanar II ECL
Neutrons (n/cm^2)		$10^{10}-10^{12}$	$10^{10}-10^{12}$	10^{14}	10^{14}	10^{13}	10^{15}	10^{15}	10^{13}	$>10^{15}$
Ionizing radiation	Total dose (rads (Si))	$>10^4$	10^4	10^6	10^6	$5\times10^4-10^5$	10^3-10^4	10^3	$>10^5$	10^7
	Transient dose rate (rads (Si)/s) (upset or saturation)	–	10^3	10^7	5×10^7	10^6	10^7	10^5	–	$>10^8$
	Transient dose rate (rads (Si)/s) (survival)	10^{10}	10^{10}	$>10^{10}$	$>10^{10}$	$>10^{10}$	10^9	10^{10}	$>10^{10}$	10^{11}
	Dormant total dose (zero bias)	$>10^4$	10^4	10^6	10^6	10^5	10^6	10^4	$>10^5$	$>10^7$

Radiation susceptibility of various semiconductors.

TABLE A4

Data source	Northrop	Sandia	Fairchild
Pulsed ionizing radiation			
Narrow pulse transient failure level	3×10^8 rads (Si)/s	no tests performed	$5-7 \times 10^8$ rads (Si)/s
Wide-pulse transient failure level	$1.1-1.4 \times 10^8$ rads (Si)/s	"	no tests performed
Permanent-damage failure level	not determined -- greater than 1.5×10^{11} rads (Si)/s	"	10^{11} rads (Si)/s maximum level (flash X-ray equipment*)
Neutron/gamma permanent damage			
Mean neutron failure level	2.2×10^{15} n/cm^2 (1 MeV equivalent)	1×10^{15} n/cm^2 (1 MeV equivalent)	1×10^{15} n/cm^2 * (1 MeV equivalent)
Total gamma dose	6.6×10^6 rads (Si)	2.5×10^7 rads (Si)	10^7 rads (Si)*
Observed neutron failure-level range	$1.9-2.6 \times 10^{15}$ n/cm^2 (1 MeV equivalent)	1×10^{15} n/cm^2 * (1 MeV equivalent)	1×10^{15} n/cm^2 * (1 MeV equivalent)
Device type tested	MC1678L 4-bit counter	custom IC fabricated by TRW	Isoplanar II, ECL F100101, F100117, F100102, F100141 and kit parts
Transistor gain-bandwidth product (f_T)	2.0-2.5 GHz	1.5 GHz	4.5-5.5 GHz

*Maximum radiation exposure level; no failures were observed at this level

Radiation susceptibility of ECL (emittor-coupled logic).

References

1) H. de Staebler, T.M. Jenkins and W.R. Nelson, "The Stanford Two-Mile Accelerator", ed. W.A. Benjamin, New York (1968).

2) D.A.G. Neet, TN-65-09 (SLAC, 1965).

3) C.J. Crannell, Phys. Rev. 161(1967)310.

4) C.J. Crannell, H. Crannell, R.R. Whitney and H.D. Zeman, Phys. Rev. 184(1969)426.

5) A. Hurkmans and R. Maas, "High-power (100 kW) slit-system", LINO-69 (IKO-Amsterdam '77).

6) B. Rossi, "High Energy Particles", Prentice-Hall Inc. New-Jersey (1956).

7) W.P. Swanson, Health Physics 35(1978)353.

8) I. Tamm and S. Belenky, J. Phys. (USSR), 1(1939)177.

9) K. Mulder, "Voorlopige berekeningen van afschermingen (EVA-II)", LINO-7 (IKO-Amsterdam '72).

10) H. de Staebler, "Transverse radiation shielding for the Stanford Two-Mile Accelerator", SLAC Report no. 9 (1962).

11) J.L. Matthews, "Neutron yields from electron beam incident on thick and thin targets", Shielding Note no. 6 (Lab. for Nucl. Sci., '67).

12) M. Pelliccioni, IEEE Trans. on Nucl. Sci., 23 no. 4 (1976)1344.

13) T.A. Gabriel and R.G. Alsmiller, Nucl. Phys. B14(1969)303.

14) R.A. Meyer, W.B. Walters and J.P. Hummel, Nucl. Phys. A122(1968)606.

15) J. Visser, "Mogelijke posities van de dump in HECH met de daarbij behorende gevolgen voor de afscherming", Intern IKO rapport, sept. '78.

16) B.L. Berman, "Atlas of photo neutron cross sections obtained with mono-energetic photons", LLL December '76 (preprint UCRL-78482).

17) W.A. Swanson, Health Physics 28(1975)495.

18) S.C. Fultz et al., Phys. Rev. B133(1964)1149.

19) M. Barber, "Induced Radioactivity", North Holland, 1969.

20) H. de Staebler, "Average radiation levels inside the accelerator housing when the machine is off", TN-62-70 (SLAC 1962).

21) Radiation Protection - Protection against electro magnetic radiation above 3 MeV and electrons, neutrons and protons", ICRP publication 4 (1963), Pergamon Press.

22) "Radiation protection design guidelines for 0.1 - 100 MeV particle accelerator facilities", NCRP Report no. 51 (1977).

23) American Institute of Physics Handbook, McGraw-Hill, 1963.

24) R.C. Mc.Call et al., SLAC-PUB-2090 (March 1978).